

Machine Learning Potentials for Heterogeneous Catalysis

Amir Omranpour,^{1,2,*} Jan Elsner,^{1,2} K. Nikolas Lausch,^{1,2} and Jörg Behler^{1,2,†}

¹*Lehrstuhl für Theoretische Chemie II, Ruhr-Universität Bochum, 44780 Bochum, Germany*

²*Research Center Chemical Sciences and Sustainability,*

Research Alliance Ruhr, 44780 Bochum, Germany

(Dated: November 4, 2024)

The sustainable production of many bulk chemicals relies on heterogeneous catalysis. The rational design or improvement of the required catalysts critically depends on insights into the underlying mechanisms at the atomic scale. In recent years, substantial progress has been made in applying advanced experimental techniques to complex catalytic reactions *in operando*, but in order to achieve a comprehensive understanding, additional information from computer simulations is indispensable in many cases. In particular, *ab initio* molecular dynamics (AIMD) has become an important tool to explicitly address the atomistic level *structure*, *dynamics*, and *reactivity* of interfacial systems, but the high computational costs limit applications to systems consisting of at most a few hundred atoms for simulation times of up to tens of picoseconds. Rapid advances in the development of modern machine learning potentials (MLP) now offer a new approach to bridge this gap, enabling simulations of complex catalytic reactions with *ab initio* accuracy at a small fraction of the computational costs. In this perspective, we provide an overview of the current state of the art of applying MLPs to systems relevant for heterogeneous catalysis along with a discussion of the prospects for the use of MLPs in catalysis science in the years to come.

I. INTRODUCTION

Heterogeneous catalysis plays an important role in many industrial processes and environmental applications by enabling chemical reactions of molecular species, which are typically in the gas or liquid phase, at solid catalyst surfaces^{1–3}. These catalysts lower activation energies, enhance reaction rates, and offer selective pathways for desired products while substantially reducing energy consumption². Some of many important examples of heterogeneously catalysed processes are, e.g., petrochemical refining⁴, ammonia synthesis⁵, hydrogenation reactions⁶, fuel cells⁷, polymerization reactions⁸, and selective oxidations^{9,10}.

Atomic-level insights into catalytic processes are essential for advancing the rational design of improved catalysts. While experimental techniques for studying catalytic reactions *in operando* have significantly advanced—using methods such as Scanning Tunneling Microscopy (STM)^{11,12}, Atomic Force Microscopy (AFM)¹¹, Sum-Frequency Vibrational Spectroscopy (SFVS)¹³, and Surface-Enhanced Raman Spectroscopy (SERS)^{13,14}—obtaining comprehensive atomic-scale information from these experiments alone remains challenging¹⁵. Thus, complementary information from theoretical studies is urgently needed. In particular electronic structure calculations, most notably Density Functional Theory (DFT), now enable the study of moderately sized systems, on the order of hundreds of atoms, with good accuracy. Consequently, to date, the most widely used theoretical approaches for investigating catalytic processes at the atomistic level are rooted in a *static* surface science

approach^{16–21}, which involves calculating the thermodynamics of surface reaction intermediates by DFT. While these methods have been very successful in screening and predicting new catalysts, they often rely on rather simple structural models of the system under study, which is sometimes referred to as the complexity gap. For instance, the solvent’s impact is often only captured implicitly or including only a small number of explicit solvent molecules, the dynamic nature of catalytic interfaces is largely ignored, and the synergistic effects of adsorbed species are not explicitly considered. Additionally, for reactions at solid-liquid interfaces the structure of a solvent near a surface exhibits significant differences compared to the bulk liquid and, e.g. in case of water, the solvent itself may undergo dissociation and recombination and can thus actively participate in reactions²². As heterogeneous catalysis increasingly involves solid-liquid interfaces—owing to their ability to operate under milder conditions and improve selectivity^{1,10}—the gap between simplified static theoretical models and real experimental conditions is becoming ever more pronounced.

In parallel to the development of electronic structure theory, various computer simulation techniques, such as Molecular Dynamics (MD)²³ and Monte Carlo (MC)²⁴, have been developed since the 1960s, which are able to account for finite-temperature effects. MD simulations, in particular, have been successfully applied to a range of biological and material systems. To effectively apply these methods—i.e., solving Newton’s equations of motion for systems with many atoms—energies and forces for a large number of structures must be computed. These can be provided in terms of atomistic potentials, which are often called force fields in biology and chemistry^{25–27}, or empirical potentials in materials science^{28–30}. However, most of these models are fitted to a narrow range of experimental or *ab initio* data sets to reproduce specific properties

* amir.omranpour@rub.de

† joerg.behler@rub.de

and thus necessarily can only reach a limited accuracy. This problem is particularly severe for catalytic systems, as not only an accurate representation of multiple bulk phases, i.e., the catalyst and the solvent exhibiting very different bonding patterns and interactions, but also of complex interfaces is required.

In 1985, Car and Parrinello proposed a method³¹ to unify MD with electronic structure calculations, laying the foundation for what is now broadly referred to as *ab initio* Molecular Dynamics (AIMD)³². AIMD offers the potential to capture the time evolution of catalytic processes and provide mechanistic insight into reaction pathways with far greater accuracy than is possible using empirical models³³. Furthermore, an important advantage of AIMD is its general applicability to a wide range of systems of different chemical compositions without the need for any system-specific adjustments. However, AIMD comes with significant computational costs, driven by the need to perform electronic structure calculations at each MD time step, which places strong limitations on both the system size and time scale accessible in the simulations. While enhanced sampling methods such as metadynamics^{34,35} and umbrella sampling³⁶ can be used to speed up the sampling of rare events that are very relevant in catalytic reactions, the cubic scaling of DFT with the number of atoms ultimately limits the complexity of system that can be handled.

Modern machine learning potentials (MLPs) allow to transfer the accuracy of first-principles electronic structure methods to large systems by constructing the high-dimensional potential energy surface based on reference electronic structure calculations for representative atomic configurations using machine learning (ML) techniques^{37–44}. This makes it feasible to run simulations for systems consisting of thousands of atoms for tens of nanoseconds, which greatly facilitates studying catalytic systems. MLPs provide a high numerical consistency with the underlying reference electronic structure method, leading to typical energy errors of around 1 meV/atom and force errors on the order of 100 meV/Å. These errors are much smaller than the uncertainties associated with different exchange-correlation functionals in DFT. Consequently, substituting direct electronic structure calculations by MLPs has only a small impact on the accuracy of the obtained results. Additionally, MLPs are inherently capable of capturing reactive events, i.e., the breaking and formation of chemical bonds, which is crucial for studying catalytic reactions. Figure 1 shows an example for a MLP-driven MD simulation of a reactive $\text{LiMn}_2\text{O}_4 \{100\}_{\text{Li}}$ –water interface⁴⁵.

Since the introduction of the first MLP in 1995⁴⁷, MLPs have now become important tools in many fields of chemistry including catalysis, and in fact chemical processes at interfaces have been a driving force in their development. As MLPs now transition from the proof-of-concept phase to mature simulation tools, this article aims to provide a perspective on their growing impact on heterogeneous catalysis research. As heterogeneous

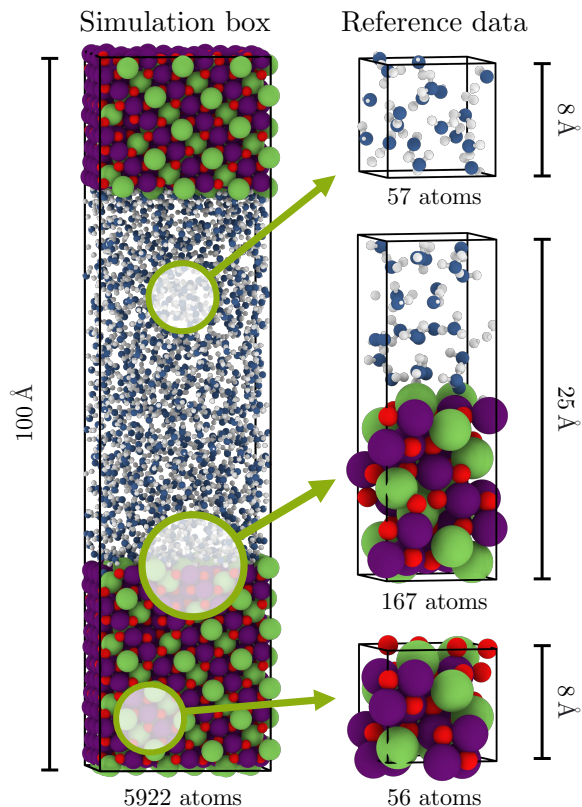


FIG. 1. Schematic representation of the $\text{LiMn}_2\text{O}_4 \{100\}_{\text{Li}}$ –water interface. On the left, the full simulation box for the final MD simulation is shown. On the right, the smaller reference systems (bulk LiMn_2O_4 , bulk water, and the $\text{LiMn}_2\text{O}_4 \{100\}_{\text{Li}}$ –water interface) used for training the MLP model are displayed. Manganese atoms are colored violet, lithium atoms green, oxygen atoms red and hydrogen atoms white. Oxygen atoms of the liquid phase are colored in blue. The figures were created using OVITO Pro (version 3.7.2)⁴⁶.

catalysis is a very broad topic, it is impossible to cover all aspects of using machine learning in this field. In this perspective, we will thus focus on its use for gaining atomic-level insights, and more specifically for representing potential energy surfaces governing catalytic reactions, which can then be used in large-scale simulations. Still, the examples discussed here can only cover some of the systems published in the literature, and other aspects and systems can be found in several related publications^{48–57}. We will not cover the more general application of machine learning techniques in heterogeneous catalysis, such as using ML to predict new catalysts bypassing the atomic level or exploring catalytic reaction networks, which are equally active fields of research^{58,59}.

This perspective is organised as follows: first, a concise overview of MLPs is provided, followed by a summary of the achievements of MLPs in elucidating different types of processes in heterogeneous catalysis. Next, several key considerations and challenges in using MLPs in catalysis are addressed, along with potential solutions to be devel-

oped. Finally, an outlook on possible future directions of the field is given.

II. MACHINE LEARNING POTENTIALS

In recent years, the development of atomistic potentials using machine learning has become a very important topic and many different methods have been proposed, each of which has its own advantages and disadvantages. In this perspective focusing on the application of MLPs in heterogeneous catalysis we do not attempt to provide a comprehensive overview of all the methodical details of MLPs, and we will just provide a bird’s eye view of the field. Instead, the interested readers are referred to several dedicated reviews addressing all the aspects of MLPs and their training in great detail^{38–44,60–68}.

Physical Classification of MLPs There are several ways to classify the many different flavors of MLPs, each focusing on different aspects. Two possible viewpoints for such categorizations are centered either on the physics governing the atomic interactions^{63,66} or take a mathematical perspective⁴³. The former, which is of particular interest for catalysis, is based on the nature and range of atomic interactions that can be described, and introduces four different generations of MLPs.

The first generation of MLPs has been restricted to very low-dimensional systems, e.g., diatomic molecules in the gas phase approaching surface models, in which the atomic positions of the surface had to be frozen to reduce the complexity of the potential energy landscape. This limitation was overcome by Behler and Parrinello with the development of high-dimensional neural network potentials (HDNNP) in 2007⁶⁹. HDNNPs introduced a decomposition of the total energy of the system into a sum of local environment-dependent atomic energy contributions E_i ,

$$E = \sum_{i=1}^{N_{\text{atom}}} E_i, \quad (1)$$

where N_{atom} is the total number of atoms in the system. Each atomic energy is then provided by machine learning, e.g., by an atomic neural network. This approach made it feasible to construct MLPs for condensed-phase systems containing large numbers of atoms such as solid surfaces central to heterogeneous catalysis. However, due to the locality approximation, interactions beyond the cutoff—typically in the range of 5 to 10 Å—are only included in an averaged manner. This class of strictly local MLPs is nowadays categorized as second-generation (2G), and many different 2G potentials are now available, which provide very accurate energy surfaces^{69–74}. However, for some systems it may be important to incorporate long-range interactions beyond the cutoff or even global phenomena like nonlocal charge transfer, for instance in some complex oxide surfaces. Overcoming these limitations is the aim of third- and fourth-generation MLPs.

In third-generation MLPs, electrostatic interactions are modeled using environment-dependent charges represented by machine learning models^{75–83}. These charges are used to compute the electrostatic energy, which is then combined with the short-range component given by Eq. (1) to yield the system’s total energy. By training the short-range component to capture only the non-electrostatic contribution to the total energy, double-counting of energy contributions is avoided. The remaining shortcomings of third-generation MLPs stem from the assumed locality of atomic charges, which makes it impossible for such models to capture long-range charge transfer that may occur in certain systems⁶⁶. Several fourth-generation MLPs have been proposed^{84–88}, which make use of global information to include these effects.

Apart from these different capabilities of MLPs to incorporate explicit physics, all MLPs inherit the intrinsic limitations of the underlying training data, in particular, the accuracy of the employed electronic structure level of theory. For instance, if certain interactions, e.g., dispersion interactions, are poorly described in DFT calculations, this will carry over to the constructed MLP. A more detailed discussion of the challenges and prospects of using MLPs to study heterogeneous catalysis will be presented in Section IV.

Classification by Representation and Learning

From the mathematical viewpoint, MLPs can be classified based on how they handle the two central tasks⁴³: (a) *representing* the structure of the system and (b) *learning* the relationship between the representation and the associated potential energy surface (PES). According to this classification, MLPs can be divided into three families:

(1) One family uses predefined descriptors in combination with nonlinear regression. This family typically employs descriptors that respect the three mandatory invariances of the atomic environment—translational, rotational, and permutational symmetries. Most of these descriptors are strictly local, defined by a specific cutoff radius. The relationship between the atomic environment descriptors and the associated PES is then learned using nonlinear fitting functions through either shallow or deep neural networks or kernel regression methods. Some typical representatives of this family include second-generation MLPs like HDNNPs⁶⁹, Gaussian Approximation Potentials (GAP)⁷⁰, and Deep Potential Molecular Dynamics (DeePMD)⁷⁴.

(2) Another family uses symmetric basis functions in combination with linear regression, albeit with non-linearity included in the basis functions. Some typical MLPs in this category are Moment Tensor Potentials (MTP)⁷³ and Atomic Cluster Expansion (ACE)⁷¹.

(3) More recently, a third family has been introduced using message-passing neural networks (MPNN)⁸⁹. In this approach, both the representation and learning tasks are addressed simultaneously. Here, the descriptors are *learned* by the neural network during training. Some examples in this category include DTNN⁹⁰, SchNet⁹¹, NequIP⁹², Allegro⁹³, and MACE⁹⁴.

In spite of the large number of MLPs that have been published to date, they have not been equally used in studies relating to heterogeneous catalysis. A review of the literature indicates that, to date, HDNNP and DeePMD are by far the most commonly applied methods in this context. However, several types of MLP, including MPNNs, have been suggested only recently, therefore it is expected that the number of studies employing these newer methods will grow substantially in the coming years.

III. APPLICATIONS TO HETEROGENEOUS CATALYSIS

A. Clusters and Surfaces

Clusters Clusters are important in catalysis, where they are commonly utilized as nanoparticles or nanoclusters to maximize the active surface area for chemical reactions. A key feature of these nanoparticles is their microstructure and morphology, which can be customized to enhance both functional properties and stability⁹⁵. Many catalysts, in fact, consist of metal clusters supported on oxides. The first applications of MLPs for metal and oxide clusters were reported for copper⁹⁶ and zinc oxide clusters⁷⁶ using HDNNPs. Further HDNNPs have been reported for Cu–Au nanoalloys employed in grand canonical MD simulations⁹⁷. For brass (Cu–Zn), HDNNP studies^{98,99} have shown that the element distribution within the nanoparticles is inhomogeneous, with zinc concentrated in the outermost layer and copper enriched in the subsurface layer. Alloying within the nanoparticle core occurs only at high zinc concentrations, forming crystalline bulk α -brass patterns. The nanoparticles’ melting temperature decreases with higher zinc content, consistent with the bulk phase behavior of brass. In Pt–Rh alloys, studies using ACE¹⁰⁰ have shown that Pt atoms segregate on the surface, forming a monolayer, which contrasts with experimental core-shell nanoclusters having thicker Pt shells that are stabilized kinetically, not thermodynamically. For Au nanoparticles, HDNNP-driven simulations¹⁰¹ revealed a rigid outer atomic layer compared to the core, where changes in surface atom coordination at around 300 K result in surface defects. The simulations also revealed a dynamic coexistence of solid-like and liquid-like phases near the melting transition. Other studies on Au^{102,103}, Pt¹⁰⁴, and Na clusters¹⁰⁵ using HDNNPs further confirm the reliability and robustness of MLP-based simulations. The dissociation of a CO₂ molecule on Cu nanoclusters was investigated using DeePMD simulations and well-tempered metadynamics¹⁰⁶, showing that the nanoclusters exhibit surface pre-melting behavior which significantly affects catalytic activity. Point defects, such as vacancies and ad-atoms were found to reduce the surface melting temperature, enabling reactions to occur under milder conditions.

Solid Surfaces The atomic environments on metal surfaces significantly differ from those in the bulk. Notably, reconstructions or imperfections on real surfaces can result in highly complex atomic configurations. Using ZnO as a case study of a multicomponent system⁷⁶, the third-generation HDNNP was introduced by incorporating environment-dependent charges to account for long-range electrostatic interactions. Copper⁹⁶ was also investigated, covering both bulk and various surface structures, including defects. The neural network potential accurately reproduced key properties such as lattice constants, cohesive energies, and surface energies. The oxidation of flat and stepped Pt surfaces, was studied using embedded atom neural network (EANN) potentials combined with grand-canonical Monte Carlo simulations¹⁰⁷, revealed the formation mechanism of the square planar PtO₄ oxide unit on a flat Pt surface.

Clusters at Surfaces Studies of copper clusters supported on zinc oxide and their extension to the ternary CuZnO system using HDNNPs^{108,109} revealed a variety of structural patterns. Exploration of copper-ceria (CuO/CeO₂) catalysts for low-temperature CO oxidation revealed that the surface-substituted Cu_yCe_{1-y}O_{2-x} phase is more catalytically active than the bulk CuO phase¹¹⁰. This was supported by *in situ* X-ray absorption spectroscopy, electron microscopy, and MLP-driven simulations, which revealed copper ion segregation to the 100 surfaces of nanoparticles. Additionally, the dynamic restructuring of 2 nm Pt nanoparticles on SiO₂ in reactive environments was studied using *in situ* spectroscopy and MD simulations with Allegro¹¹¹, revealing that nanoparticle surfaces lose their atomic order when exposed to CO gas, while their cores remain bulk-like. This challenges traditional models that assume idealized faceting, highlighting the need for models that account for realistic surface structures to predict catalyst function and stability.

B. Solid-Gas Interfaces

Early MLPs Since the early days of MLPs, their development was motivated by the challenge of accurately representing the PES for gas-surface dynamics. Before the breakthrough of MLPs, extensive work during the 1990s and early 2000s focused on analytic PESs for gas-surface dynamics, employing many different approaches^{112–117}. A primary limitation of these analytic PESs was their restriction to six dimensions for diatomic molecules on surfaces. Additionally, simulating chemical reaction probabilities, particularly in gas-surface dynamics, demands a precise mapping of energy landscapes. Even minor errors in reaction barriers can lead to significant deviations in predicted reaction probabilities, posing an additional challenge for PES representation.

In response to these limitations, Blank et al.⁴⁷ introduced the use of neural networks as a general, nonlinear fitting approach that avoids assumptions about the po-

tential energy surface topology. This approach, using a limited set of data points, demonstrated the ability to model complex chemical interactions with high accuracy. It showed, for the first time that feed-forward neural networks can accurately model PESs, outperforming traditional methods like splines. This technique was applied to systems such as CO on Ni(111) and H₂ on Si(100), providing precise predictions of the potential energy.

In 2004, Lorenz et al.¹¹⁸ took the next step by further reducing the number of training points by exploiting the underlying surface symmetries in periodic slabs. They demonstrated the accuracy and efficiency of neural network potentials (NNPs) for H₂ interacting with the (2×2) potassium-covered Pd(100) surface. The sticking probability of H₂/K(2×2)/Pd(100) was determined by MD simulations on the neural network PES and compared to results obtained using an independent analytical interpolation. It was shown that, by accounting for the symmetries underlying the particular system and incorporating feedback from dynamical simulations, a relatively moderate number of training points is needed to obtain a reliable fit¹¹⁹.

Similar methodologies were employed by Behler et al. to study O₂ dissociation on Al surfaces¹²⁰. Symmetrized functions were introduced¹²¹ to fully account for the surface’s symmetry and nonadiabatic effects were also investigated¹²². Instead of molecular coordinates, the symmetrized functions, systematically constructed from atomic Fourier terms, were used as inputs to the neural network. This approach was validated for O₂ interacting with the Al(111) surface. Building on this work, additional studies for O₂ dissociation on Al were conducted by Carbogno et al.^{123,124}.

O₂ adsorption on Ag surfaces was also investigated¹²⁵ and it was shown that the dissociation probabilities match experimental data, suggesting that the surface’s inertness is primarily due to energy barriers, with spin or charge nonadiabaticity playing a negligible role. Later, the conventional view that physisorption states significantly influence molecular scattering experiments was challenged¹²⁶. Despite the inability of semilocal DFT to accurately capture long-range van der Waals interactions and the absence of physisorption wells, experimental scattering trends were successfully reproduced in the simulations. It was suggested that molecular scattering is more influenced by the repulsive walls associated with chemisorption rather than by physisorption, casting doubt on the use of scattering data as indirect evidence for the existence of physisorption states.

Ammonia Decomposition The work discussed so far represents initial efforts employing first-generation MLPs. Since then, MLPs have reached a level of maturity that allows them to be used to study some of the key challenging systems in catalysis, such as the Haber-Bosch process for ammonia synthesis⁵, which is essential for producing fertilizers and sustaining global food production. Traditionally, theoretical modeling at *operando* industrial-level temperatures was unfeasible, often re-

lying on extrapolations from lower-temperature results. However, the validity of this approach has been recently questioned by a series of works by Parrinello et al.^{127–130}. In particular, these studies directly highlight the role of dynamics in ammonia decomposition on the iron surface relevant to the Haber-Bosch process.

In the Haber-Bosch process, the rate-limiting step is believed to be the N₂ decomposition on Fe catalysts, due to the strong triple bond of N₂ molecules. N₂ decomposition on Fe(111) was investigated¹²⁷ using DeePMD and metadynamics simulations, revealing the disruptive effect of dynamic changes on the Fe(111) surface morphology, which significantly influences nitrogen adsorption and dissociation, particularly at elevated temperatures. The study highlights the risk of extrapolating low-temperature results to *operando* conditions (700 K for the N₂ decomposition), due to the nonlinearity of catalytic behavior with temperature, and demonstrates that catalytic activity can only be accurately inferred from simulations that explicitly account for dynamics. Additionally, it has been shown¹²⁸ that ammonia decomposition over a wustite-based bulk iron catalyst results in the formation of iron nitrides (Fe₄N and Fe₂N) at lower temperatures. The decomposition of Fe₄N into Fe and N₂ was identified as the rate-determining step, with activation energies of 172 and 173 kJ/mol, respectively. MD simulations demonstrated that nitrogen migration into the bulk of the catalyst is favored over recombination at the surface, significantly impacting the efficiency of nitrogen desorption and nitride formation.

Al₂O₃(0001) Surface The Al₂O₃(0001) surface is important in catalysis as it serves as a stable support material for dispersing active catalytic species, enhancing activity and durability. Its well-defined atomic structure and low reactivity make it suitable for high-temperature catalytic processes, while its surface properties allow for controlled adsorption and surface reactions, making it valuable for studying heterogeneous catalysis. The stoichiometric reconstruction of the Al₂O₃(0001) surface—considered one of surface science’s mysteries¹³¹—was recently investigated¹³² using noncontact atomic force microscopy (nc-AFM) and DFT calculations enhanced by VASP’s on-the-fly MLPs^{133–135}, based on GAP. Imaging revealed the lateral atomic positions, while theoretical analysis indicated that aluminum rehybridization enables bonding with subsurface oxygen atoms, significantly stabilizing the reconstruction. In another study using an HDNNP, hydrogen atom scattering at the Al₂O₃(0001) surface was examined¹³⁶. The best agreement between experimental atom beam scattering and theory occurs at large initial kinetic energies and at both very low and high scattering angles, attributed to scattering from top-layer aluminum atoms. In contrast, lower initial kinetic energies result in greater kinetic energy loss in the MD trajectories compared to experiment. Additionally, scattering at oxygen sites generally leads to larger discrepancies.

Other Gas-Surface Systems Numerous other stud-

ies have employed MLPs to model gas-surface dynamics. For instance, NNPs have been employed to investigate H_2 dissociation on Pt(111) and Cu(111), demonstrating that reduced energetic corrugation broadens the reaction probability curve¹³⁷. In a combined HDNNP and STM study¹³⁸, it was found that high CO coverage at a Pt step edge induces the formation of atomic protrusions composed of low-coordination Pt atoms. These atoms then detach from the step edge, forming sub-nano-islands on the terraces, where the CO adsorbates stabilize the under-coordinated sites. H_2 dissociation on Pt(111) was also examined using an on-the-fly trained Sparse Gaussian Process (SGP) potential¹³⁹, while H_2 dissociation on curved Pt surfaces was studied with HDNNPs¹⁴⁰.

Investigation of N_2O dissociation on Cu(100)¹⁴¹ showed that N_2O initially weakly adsorbs on Cu(100) before reaching a stable chemisorbed state at a hollow site, with dissociation into N_2 and adsorbed oxygen becoming favorable at higher translational energies. Vibrational shifts in adsorbed N_2O reflect bond weakening, facilitating dissociation, while changes in rotational temperature have minimal effect on this process. The quantum mechanics/molecular mechanics (QM/MM) embedding method for O_2 on Pd(100), where a NNP was used to surrogate DFT calculations, revealed significant energy release during dissociation. This release resulted in highly mobile oxygen atoms, challenging the assumption of instantaneous thermalization in catalytic processes¹⁴². NNP-based studies of HCl on Au(111)¹⁴³ showed that the RPBE functional produces higher reaction barriers and lower probabilities than PBE, improving agreement with the experiment, while reactivity is highly sensitive to the rovibrational state population. Surface atom motion, nonadiabatic effects, and moderate charge transfer at the transition state influence the reaction only modestly. A 15-dimensional PES for CH_4 on Ni(111) was found to accurately reproduce methane dissociation dynamics, providing valuable insights for industrial applications¹⁴⁴. Additionally, the use of the Allegro architecture⁹³ combined with enhanced sampling techniques revealed a dynamic interplay between CH_4 and the Ni catalyst, highlighting the increased mobility of adsorbed species, especially at higher temperatures¹⁴⁵.

The interactions of N_2 with Ru(0001) were explored using an HDNNP trained on RPBE data, showing agreement with experimental molecular beam sticking probabilities¹⁴⁶. Further analysis revealed that vibrational excitation is more efficient than translational energy in overcoming activation barriers¹⁴⁷. HDNNPs were also able to provide accurate reaction probabilities for the highly activated reaction of CHD_3 on Cu(111)¹⁴⁸, the effect of orbital-dependent electronic friction on the description of reactive scattering of N_2 from Ru(0001)¹⁴⁹, and H-atom on free-standing graphene¹⁵⁰. For oxygen on Pd surfaces, HDNNP models were able to predict adsorption energies and diffusion barriers accurately, though improvements are needed at high coverages due to surface reconstructions¹⁵¹. Hydrogen scattering on copper sur-

faces has also been evaluated using various MLP models.^{152,153} A study of CO on Ru(0001) using EANN potentials¹⁵⁴ offered strong support for describing both photoinduced desorption and CO oxidation through nonequilibrium, yet thermal, hot electrons and phonons. The MACE potential was applied to investigate ammonia decomposition on iron-cobalt alloy surfaces¹⁵⁵.

C. Solid-Liquid Interfaces

Solid-liquid interfaces are of constantly increasing importance in heterogeneous catalysis and electrocatalysis. Even pristine surfaces in contact with pure water display significant complexity due to the active role of interfacial water molecules, which may undergo dissociation and recombination — particularly on transition metal oxides. An accurate description of the interface therefore requires an explicit description of water that also captures reactivity.

Early work on solid-liquid interfaces using HDNNPs investigated the effect of solvation on the surface composition of Au-Cu nanoparticles¹⁵⁶. When solvent water molecules were included, a mixed Au-Cu surface was preferred, while a core-shell structure was predicted in a vacuum. Soon after, the question of how much water is needed to achieve bulk-water-like behavior at various prototypical Cu-water interface models was addressed using an HDNNP¹⁵⁷. It was found that a water film thickness of at least 40 Å is required to prevent artificial interactions between opposing surfaces and to ensure bulk-like properties in the central region of the water film — a scale that is computationally prohibitive for *ab initio* models.

Much attention has been given to the extent of water dissociation and proton transfer (PT) mechanisms at oxide-water interfaces. The first MLP-based studies of this kind focused on ZnO-water interfaces^{158–161}. Simulations of the ZnO(10 $\bar{1}$ 0)¹⁵⁸ and ZnO(11 $\bar{2}$ 0)-water interfaces¹⁶⁰ using an HDNNP revealed two dominant types of interfacial PT reactions: PT between surface oxygen atoms and adsorbed hydroxide ions (surface-PT), and PT between adsorbed water molecules and neighbouring adsorbed hydroxide ions (adlayer-PT). Notably, fluctuations in the local hydrogen-bonding environment were found to have a significant effect on PT barriers and corresponding rates¹⁵⁸. The influence of surface proximity and local hydrogen bonding network on the anharmonic OH stretching vibrations of water and hydroxide ions near the interface were also investigated at the ZnO(10 $\bar{1}$ 0)-water interface¹⁵⁹. A representative snapshot of this system is shown in Figure 2, where approximately 70 % of surface oxygen sites are hydroxylated with protons arising from dissociated water¹⁵⁸.

Consecutive proton transfer reactions at the interface can lead to long-range Grotthuss-like proton diffusion. This was investigated at the ZnO(10 $\bar{1}$ 0) and (11 $\bar{2}$ 0) facets, which showed very different behaviour: proton-diffusion on ZnO(10 $\bar{1}$ 0) was found to be quasi-

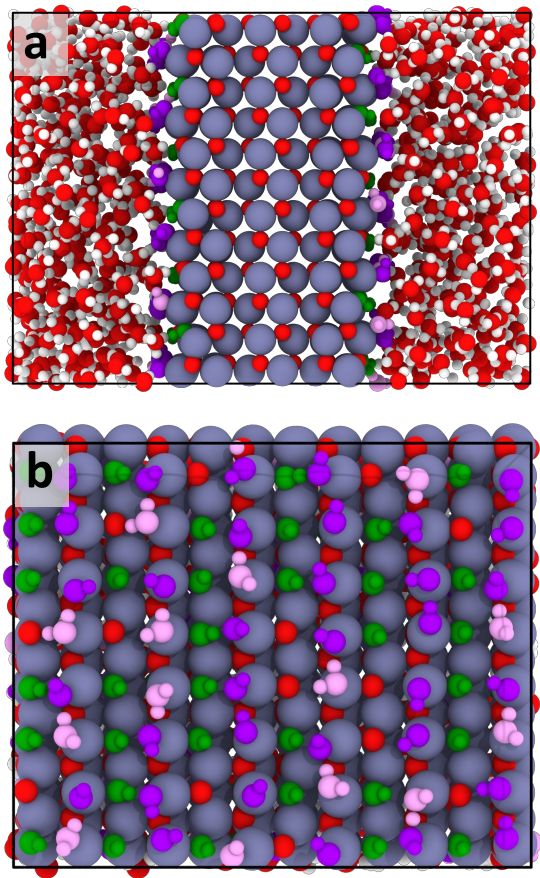


FIG. 2. Snapshots of the ZnO(10 $\bar{1}0$)-water interface, illustrating the presence of dissociated water at the surface. (a) Side view of the interface model. (b) Top view displaying only the first layer of adsorbed and dissociated water. Adsorbed water molecules, adsorbed hydroxide ions and surface hydroxyl groups are colored in light pink, purple and green, respectively. Hydrogen atoms are assigned to their nearest oxygen atom, while adsorbed species are defined as those with oxygen atoms within 2.5 Å of a surface zinc atom.

one-dimensional, whereas on ZnO(11 $\bar{2}0$) two-dimension proton transfer was observed¹⁶¹. These differences highlight the strong influence of surface morphology on proton transport pathways. Similar observations have been reported in a recent study on long-range proton transport at the CeO₂(111) and (110)-water interfaces using DeePMD simulations, which demonstrated significantly more active proton transport on the (111) facet compared to (110)¹⁶².

MLPs have been used extensively to study the water interfaces of TiO₂^{163–169}, an important system for photocatalysis^{170,171}. At the TiO₂ anatase(101)-water interface, DeePMD simulations showed a relatively small extent of water dissociation, ~6 %¹⁶³. Employing umbrella sampling simulations to compute the free energy

surface for water dissociation, it was shown that molecularly adsorbed water is significantly more stable than dissociated water with a large free energy barrier. Water dissociation is therefore only observed on timescales longer than those accessible with AIMD. Subsequent DeePMD-based investigation of this system in conjunction with infrared spectroscopy revealed significant restructuring of the hydrogen bonding network as water coverage increased, transitioning from 1D chains at monolayer coverage to 2D and 3D networks at higher coverages¹⁶⁵. Non-equilibrium MD simulations of thermal transport across the TiO₂ anatase(101)-water interface using DeePMD have highlighted the important role of water dissociation on the interfacial vibrational density of states (VDOS)¹⁶⁶. Using empirical potentials instead, which do not capture water dissociation, resulted in higher interfacial thermal conductance due to substantial differences in the interfacial VDOS. Similar simulations were carried out for the copper-water interface¹⁷².

At the TiO₂ rutile(110)-water interface, odd-even oscillations in the surface hydroxylation level with respect to the number of O-Ti-O trilayers have been observed in DeePMD studies^{167,168}. Similar oscillations were identified in ab initio studies¹⁷³, though computational expense limited these investigations to thin slabs and low water coverage. A PBE+D3-based MLP resulted in an average hydroxylation fraction of 2 % for thick slabs¹⁶⁷, whereas a SCAN-based MLP resulted in a notably higher value of 22 %¹⁶⁸. These discrepancies likely stem from the different density functionals underlying the respective potentials. Water dissociation was found to proceed via two possible mechanisms; direct proton transfer and indirect transfer via a solvent molecule¹⁶⁸, which differs from anatase(101), where the direct mechanism was not observed¹⁶³ due to the larger distance between adjacent surface Ti and O sites. To paint a more general picture of TiO₂-water interfaces, seven different low-index TiO₂-water interfaces were jointly investigated with HDNNPs¹⁶⁹. Here, free energy surfaces from metadynamics simulations revealed that water dissociation is thermodynamically favourable on anatase(100), anatase(110), rutile(001), and rutile(011), whereas molecular adsorption is favoured on anatase(101), rutile(100) and rutile(110). Surface dependent activity was also observed in DeePMD simulations of the TiS₂-water interface, where water dissociation was observed on only one of four investigated surfaces¹⁷⁴. Here, free energy profiles from umbrella sampling simulations showed this to be the only surface where water dissociation was thermodynamically and kinetically favourable, which was attributed to the unique presence of both four-fold-coordinated Ti and one-fold-coordinated S surface atoms.

Some oxides feature a particularly complex electronic structure, where metal ions exist in multiple oxidation states. This is the case for LiMn₂O₄, whose interfaces with water were investigated using an HDNNP⁴⁵. Here, Mn ions coexist in the Mn^{IV} and high-spin Mn^{III} ox-

dation states, necessitating the use of a hybrid density functional to obtain the correct oxidation state distribution. Notably, the valency of the manganese ions has been linked to LiMn_2O_4 's water oxidation properties¹⁷⁵. Even though HDNNPs do not include explicit information on the electronic structure, it was shown that this information is learned implicitly and the oxidation state distribution at the surface could be recovered from the predicted dynamics. The oxidation state distribution and water dynamics at the interface, including water dissociation and proton transfer reactions, were found to differ significantly between the investigated surface orientations and terminations.

MLPs have also been used to investigate solvation dynamics at the hematite(001)-water interface¹⁷⁶, proton transfer mechanisms at the water interfaces with GaP(110)¹⁷⁷, as well as ice nucleation on microcline feldspar¹⁷⁸ and the dynamics of surface K^+ ions at the muscovite-water interface^{179,180}. DeePMD, in conjunction with Deep Wannier models^{181,182} for the prediction of atomic dipole moments and polarizabilities, has been employed to investigate the interfacial water structure at the $\alpha\text{-Al}_2\text{O}_3$ (0001) surface through computational Sum-Frequency Generation (SFG) spectroscopy¹⁸³. At the water interfaces of IrO_2 (110)¹⁸⁴ and SnO_2 (110)¹⁸⁵, proton transfer mechanisms and acid-base equilibrium properties were investigated, including the calculation of pKa values from calculated free energy differences based on enhanced sampling simulations¹⁸⁴ and a counting analysis¹⁸⁵. Alternatively, thermodynamic integration may be used to compute pKa values. Recent studies have demonstrated the utility of MLPs in this context for aqueous molecules¹⁸⁶ and transition-metal complexes¹⁸⁷ with DeePMD, and for BiVO_4 in water using a committee of HDNNPs¹⁸⁸.

Theoretical models of the Pt-water interface have been of great interest for a long time due to the frequent use of Pt electrodes in electrocatalysis. HDNNP-based MD simulations of the Pt(111)-water interface showed the formation of a double layer¹⁸⁹. However, unlike the ordered bilayer that was assumed to form under ultra-high vacuum conditions, the interfacial water structure was found to be dynamically changing due to repulsive interactions between adsorbed water molecules, leading to a semi-ordered structure. The transfer time of water molecules from the secondary water layer to the surface was found to be around 30 ps, while transfer from the water bulk takes 500 ps, far exceeding the timescales accessible using DFT. When comparing the coverage dependence of hydroxyl adsorption between the conventional bilayer and explicit water model, a different trend was observed at large coverage, where explicit solvent molecules were found to significantly reduce the adsorption barrier¹⁹⁰. Furthermore, the effect of steps at the Pt(211) surface on the properties of the interfacial water has been investigated using DeePMD¹⁹¹, revealing distinct physi- and chemisorption patterns and anisotropic dynamics along steps. Recent work investigating con-

tact layer water at various surfaces, including Pt, Au, graphene, and MoS_2 , has highlighted notable differences in the short-range anisotropy and long-range homogeneity of the oxygen-oxygen pair correlation functions of water at these surfaces¹⁹². These variations were found to impact phenomena such as nanofluidic slip and diffusio-osmotic transport, with the in-plane corrugation of the contact layer playing a key role.

Imperfect Surfaces In experiment, surfaces are rarely pristine. Capturing the complexity of realistic surfaces in interface systems is challenging, since the precise nature of defects in experiment is often not known. MLP-driven simulations can provide valuable insight which may help to identify the nature of defects and their properties. For instance, recent electrochemical scanning tunnelling microscopy experiments revealed a double-row pattern in the structure of interfacial water at the TiO_2 rutile(110)-water interface¹⁹³. DeePMD simulations were able to quantitatively reproduce the experimental pattern, but only after a $[\bar{1}\bar{1}1]$ step was included in the computational model¹⁹³. Thus, the simulations point to the presence of $[\bar{1}\bar{1}1]$ steps on this surface. Modelling stepped surfaces of this kind requires thousands of atoms, rendering ab initio MD unfeasible.

To date, only a few MLP-driven studies of solid-liquid interfaces have considered non-pristine surfaces. In relatively early work, the diffusion of surface adatoms and vacancy defects at low-index and stepped Cu-water interfaces was investigated using HDNNPs¹⁹⁴. Free energy profiles for adatom and vacancy diffusion from metadynamics simulations were compared to barriers obtained from nudged-elastic-band (NEB) calculations in vacuum, revealing that solvation significantly affects barrier heights for adatom diffusion but has only a marginal impact on vacancy diffusion. Water adsorption on MgO and magnetite surfaces, including step and line defects for the latter, has been investigated using VASP's on-the-fly MLPs, based on GAPS¹⁹⁵. Defect segregation and the impact of oxygen vacancies at zirconium oxide- and oxynitride-water interfaces have been investigated using MLP-driven Monte Carlo (MC) simulations, showing that water adsorbs preferably at zirconium sites surrounded by vacancies but not on the vacancies themselves¹⁹⁶.

Amorphous systems have shown promise as heterogeneous catalysts, sometimes even outperforming their crystalline counterparts¹⁹⁷. The amorphous TiO_2 -water interface has been investigated with DeePMD¹⁹⁸, showing that interfacial water is far more disordered than observed for crystalline facets, resulting in a ~ 10 fold increase in the diffusivity of interfacial water molecules compared to the rutile(110)¹⁶⁸ and anatase(101)-water interfaces¹⁹⁹.

Surface reconstruction has been investigated at perovskite oxide-water interfaces using VASP's on-the-fly MLPs²⁰⁰. Here, oxygen exchange from the lattice to the liquid, facilitated by the relatively weak Co-O bond, was found to lead to the formation of surface peroxy

species and O_2 gas, suggesting that Co atoms may act as active sites for the oxygen evolution reaction. Recently, the Subsurface Cation Vacancy (SCV) model of the magnetite(001)/water interface, where subsurface cation vacancies stabilize the reconstructed surface²⁰¹, has been investigated with HDNNPs²⁰², uncovering new low-coverage water ground states and anisotropic diffusion of water on the surface.

Nanoconfined Systems Nanoconfinement has been shown to significantly affect the performance of electrocatalysts²⁰³. Understanding the effect of confinement at the atomistic scale can provide valuable insights for optimizing the design and implementation of nanoconfined systems in electrocatalysis. HDNNPs have been used to investigate water permeation between stacked layers of hexagonal boron nitride (hBN)²⁰⁴, revealing a significant increase in the water self-diffusion coefficient under strong confinement—a result not captured by simpler water models such as SPC/E or TIP4P due to a poor description of water-surface interactions. Studies of nanoconfined water between graphene sheets using DeePMD^{205,206} have shown an increase in water permeability under confinement. From experiment, it is known that water transport is significantly faster in graphene nanotubes compared to hBN. However, the origin of this behavior was not well understood²⁰⁷. HDNNP-based investigation of these systems could reproduce the experimental trend, and provide atomic-scale insight into the different water transport properties of these systems²⁰⁸. Hydrogen atoms from water were found to interact strongly with nitrogen atoms at the hBN surface, leading to substantial residence time and slow transport. Such interactions are not present for graphene nanotubes, leading to faster transport dynamics. Finally, DeePMD investigation of nanoconfined water between TiO_2 anatase(101) slabs showed the formation of 1D water chains on the surface, leading to anisotropic surface hydrogen diffusion, as well as significantly reduced surface hydroxyl lifetimes²⁰⁹.

Beyond Pure Water Given the complexity of structural motifs and reactivity of even pure water at a solid surface, few studies have considered additional species at solid-water interfaces so far. Including reactants in simulations of solid-liquid interfaces is, of course, crucial for extending these studies to real catalytic processes, making this an important area for future research.

The effect of explicit solvents on adsorbate properties at the Cu(111)-water interface has been investigated with MLPs²¹⁰. Binding energies of CO and OH obtained using implicit vs. explicit solvent models showed significant discrepancy, particularly for OH, which actively participates in the hydrogen bonding network. Metadynamics simulations were used to compute the free energy barriers for C–H bond breaking of ethylene glycol over Cu(111) and Pd(111), revealing distinct reaction pathways on the two surfaces, with bond breaking occurring more readily on Pd(111).

The oxygen reduction reaction (ORR) at the Au(100)-

water interface has been investigated with metadynamics simulations²¹¹ employing the message-passing graph neural network PaiNN²¹². An O_2 molecule introduced into the liquid phase was found to readily migrate to the surface. The ORR was shown to proceed via an associative reaction pathway with a low barrier of 0.3 eV, consistent with experimental observations of high ORR activity on Au(100), but showing slight mechanistic differences from the pathway proposed in earlier theoretical work²⁰.

Protonated water confined between MXene sheets, a class of 2D transition metal carbides or nitrides with applications in (photo)catalysis²¹³, has been studied using DeePMD simulations²¹⁴. The presence of Eigen and Zundel cations was found to influence the orientation of nearby water molecules, which in turn inhibited water-induced oxidation of the surface, a process previously identified in DeePMD simulations of the MXene interface with pure water²¹⁵. Additionally, an unusual hexagonal ice phase, stabilized by hydrogen bonds to the MXene surface, was observed for low proton concentrations at room temperature.

Moreover, the behavior of carboxylic acids at the TiO_2 anatase(101)-water interface has been investigated with DeePMD simulations²¹⁶. At high acid coverage, a transition from bidentate to monodentate adsorption was observed, accompanied by the co-adsorption of a water molecule on the vacated Ti_{5c} site. This configuration was found to be stable over long timescales, which could not be observed in shorter AIMD simulations. Furthermore, the effect of varying the pH of anatase(101)-electrolyte solutions has been investigated with DeePMD simulations²¹⁷. Here, a Deep Wannier model was trained to reproduce DFT Wannier centers, enabling the calculation of the electrostatic potential profile and interfacial capacitance. The results highlight the complexity of the ion distribution at solid-electrolyte interfaces which is not captured by mean-field theories such as the Gouy-Chapman-Stern (GCS) model²¹⁸. For instance, positively charged counterions were found to approach the surface more closely than negatively charged counterions due to the electronegative surface oxygen atoms, regardless of the pH and surface charge. Consequently, the interfacial capacitance was found to be larger for basic solutions with negative surface charge compared to acidic solutions with positive surface charge, consistent with experiment²¹⁹ but in contrast to the GCS prediction.

The additional complexity introduced when adsorbates are included at solid-liquid interfaces presents a challenge, requiring more exhaustive training to fully capture the configuration space. To tackle this, a hybrid QM, FF, and MLP approach was recently proposed for computing aqueous-phase adsorption free energies. Here, an MLP is used only for water-surface interactions, while water-water and adsorbate-surface interactions are treated at different levels of theory²²⁰. This approach retains some of the speedup advantages of MLPs, while simplifying the active learning problem since the MLP

needs only to cover a subset of the full configuration space.

IV. DISCUSSIONS, CHALLENGES, AND OUTLOOK

The broad application of MLPs discussed in the previous section demonstrates that MLPs have matured beyond their initial proof-of-concept phase to the point where the investigation of realistic catalytic systems is now possible. From metal clusters and solid surfaces to gas-surface dynamics and solid-liquid interfaces, MLPs are becoming ubiquitous tools in the theoretical study of catalytic processes. However, the construction and application of MLPs, particularly in heterogeneous catalysis, requires great care, since ML models are, to some extent or entirely, agnostic to the underlying physics of the system, learning the shape of the potential energy surface from the data provided. This flexibility, while offering a significant advantage over empirical potentials, demands caution, i.e., they are still far from being a black-box solution. In the following, several key considerations concerning the use of MLPs in heterogeneous catalysis are discussed.

Reference Configurations and Data Efficiency

To train MLPs, reference configurations along with their associated energies, forces, and possibly charges, spins and stresses, must be provided. However, selecting the most relevant configurations is nontrivial, as they should ideally encompass the atomic environments likely to be encountered in the target simulations. Predicting all such relevant environments beforehand is practically impossible. Including as many relevant structures as possible improves the accuracy and reliability of the MLPs. However, this raises concerns about data efficiency. Due to the computational cost of reference electronic structure calculations and the demands of training on large datasets, minimizing the amount of data required to build the MLP is crucial. This is particularly important for catalytic systems, where the training data must not only include bulk solid and liquid phases but also complex interfaces (see Figure 1).

These challenges may be addressed with active learning schemes^{68,96,139,155,221}. Active learning is an iterative process that enhances MLP accuracy by selectively improving underrepresented parts of the configuration space. One common approach is query by committee (QbC)²²¹⁻²²⁴, where the variance in energy (or force) predictions across an ensemble (or “committee”) of similarly-trained models is used as a measure of uncertainty. Structures with large committee variance, which are thus underrepresented in the training set, can be identified as important data points to include in further training cycles. A partially trained committee model may be used to drive MD simulations at the intended production conditions. In this way, the relevant configuration space is

explored autonomously. When high-uncertainty configurations are encountered, additional reference calculations can be performed and added to the dataset, followed by retraining the MLP. This process can be repeated over multiple iterations, until the configuration space of interest is sufficiently well sampled.

Schemes to identify reaction coordinates and improve the sampling of rare transitions in complex molecular systems have also been proposed²²⁵⁻²²⁷. Another approach to enhance data efficiency involves using equivariant descriptors, which have been shown to significantly reduce the amount of training data required⁹². This approach is part of a broader design philosophy that advocates *exploiting* the symmetry operations in 3D space, rather than merely *respecting* them²²⁸⁻²³⁰.

Transferability The concept of *transferability* is used with varying meanings and in different contexts in the literature. In the context of empirical potentials, which are inherently fitted to a limited number of experimental or high-quality quantum mechanical data, transferability usually refers to the potential’s ability to reproduce properties of systems not included during its construction. This issue is somewhat mitigated in MLPs since they are trained on the potential energy surface itself rather than specific properties or parameters. However, MLPs perform poorly when applied outside the configuration space covered during training.

Active learning, discussed in the preceding section, can be used to systematically extend the model to accurately cover new thermodynamic (or compositional) state points, however this requires some effort if many such state points are of interest. Some recent graph neural networks have shown impressive extrapolation abilities beyond the training dataset, however such claims must be approached with caution, and further evaluations are needed to verify their reliability. Another promising approach is to utilize transfer learning and foundation models as initial frameworks for MLP development, which could potentially improve transferability and out-of-distribution performance^{231,232}.

Reference Electronic Structure Method Although MLPs are not restricted to any specific electronic structure technique, DFT, particularly at the GGA level of theory, remains the workhorse for heterogeneous catalysis. This is because the complexity of catalytic interfaces typically requires thousands of electronic structure calculations on systems large enough to include the bulk catalyst, solvents, and their interfaces in the training dataset. However, GGA functionals suffer from several limitations, such as self-interaction error, resulting in underestimated band gaps, as well as inaccurate prediction of reaction barriers and structural properties. These shortcomings are particularly pronounced in systems with localized or strongly correlated electrons such as transition metal oxides. Moving beyond GGA functionals can help mitigate these issues by incorporating additional information, such as kinetic energy density in meta-GGAs or exact exchange from Hartree-Fock theory in hybrid func-

tionals, leading to more accurate and reliable predictions. Additionally, corrections for missing dispersion interactions are often required, especially for systems including water²³³. While beyond-DFT methods have already been employed to construct MLPs for bulk systems, for example using coupled-cluster theory for liquid water^{234–236} and the random-phase approximation (RPA) for zirconium oxide²³⁷, it seems unlikely that these methods will become mainstream for studying catalysis in the near future for most practical applications. However, this trend may change with increasing efficiency of electronic structure calculations.

The choice of DFT functional for constructing the training dataset must be considered carefully. A well-established procedure for verifying the suitability of a given functional is to benchmark the description of experimentally accessible observables e.g., slab lattice parameters, solvent density, or surface adsorption energies in the case of solid-gas interfaces, against experimental results or data from higher levels of theory. Multi-component systems generally pose an increased challenge, as some GGA functionals are known to better describe solvents, while others might be better suited to describe solids. Transition metal oxide systems²³⁸, for example, are often well described by PBE-based hybrid functionals such as HSE06 or PBE0, but their weak description of water is well-documented.²³⁹ The inefficacy of DFT, particularly GGA functionals, in describing the adsorption of molecules on catalysts is also well-known. However, a detailed discussion of the advantages and disadvantages of various functionals and electronic structure techniques is beyond the scope of this article. For further information, the reader is referred to more detailed reports on the subject (see Ref. 240). To conclude, in practice, when generating the reference data for a catalytic system the electronic structure method that can describe the overall system at the desired accuracy has to be chosen with great care while the method also still needs to be efficient enough to enable a sufficient sampling of the relevant configuration space.

Accuracy Comparing the accuracy of different MLP models is a complex task. For instance, while MLP A may outperform MLP B on a specific dataset, it could underperform on another, making it challenging to find a balanced comparison between MLPs in the literature, though some initial attempts have been made^{152,153,210}. The current practice for evaluating new MLP models involves comparing their energy and force root mean square errors (RMSE) on benchmark datasets. However, it has been shown that although such evaluations are necessary, they are not sufficient^{241,242}. It is important to note that most state-of-the-art MLP implementations generally achieve energy errors around 1 meV/atom and force errors on the order of 100 meV/Å. These error magnitudes are significantly smaller than the uncertainties introduced by factors like the choice of exchange-correlation functional in DFT. Furthermore, studies have demonstrated that the discrepancy between DFT and

experimental observables is greater than that between MLPs and DFT^{243,244}. Since MLPs are inherently limited by the accuracy of the underlying electronic structure methods, a practical recommendation when applying MLP models to heterogeneous catalysis is to prioritize generating high-quality reference data using the most accurate electronic structure methods and ensuring convergence, rather than over-investing on the selection of a particular MLP.

Long-Range Interactions Most MLPs are local, i.e., they construct the potential energy surface as a sum of environment dependent atomic energy contributions. However, some interactions, such as dispersion or electrostatics, can reach far beyond the typical cutoff range of 5 to 10 Å. During training, the tail of these interactions is not truncated but partitioned into the local atomic environments. For most condensed phase systems this approach is sufficient because these interactions are effectively screened and therefore, the contribution beyond the cutoff is very small. However, when they are still significant, they act like noise during training, which can reduce the quality of the fit.²⁴⁵ In condensed phase systems containing e.g., electrolytes or ionic liquids, or solid-gas interface systems, where screening effects are significantly reduced, an explicit treatment of long-range interactions can therefore become necessary to achieve the desired accuracy.²⁴⁵

MLPs of the third and fourth generation have been extended to include long-range electrostatics by learning environment dependent charges from which electrostatic energies and forces can be computed. Similarly, long-range dispersion corrections such as the Tkatschenko-Scheffler²⁴⁶ and exchange-hole dipole moment^{247,248} model have been combined with MLPs by learning environment dependent Hirshfeld volumes,²⁴⁹ and Hirshfeld volumes and exchange-hole moments²⁵⁰. Additionally, long-range dispersion can also be included without falling back on an additional ML model by applying Grimme’s geometry dependent DFT-D3 correction²⁵¹.

Non-Local Interactions For many systems, accounting only for local interactions is sufficient to achieve an accurate description.⁸⁸ However, for some systems, accounting for global interactions becomes necessary to predict the correct dynamics. Ko et al.⁸⁶ demonstrated that using a model containing an Au₂ cluster supported on a MgO substrate. On pristine MgO, the Au₂ cluster takes an upright configuration where only a single Au atom is adsorbed to the surface. Introducing Al doping, which replaces some Mg sites below the surface, leads to a global charge redistribution and different optimal Au₂ cluster configuration that is parallel to the surface where both Au atoms directly interact with the surface. In this model the doping is introduced at a distance beyond the cutoff. Consequently, local MLPs are unable to predict the change in adsorption geometry of the Au₂ cluster when introducing the dopant. Using a 4G-HDNNP, Ko et al. are able to predict the correct adsorption geometry. Unke et al.⁸⁸ also demonstrated that their proposed

MPNN architecture SpookyNet, that includes nonlocal interactions, is able to describe this model accurately.

Electrode Potentials and External Electric Fields In a realistic electrochemical setting, reactions normally occur under a constant electrode potential. This requires free exchange of electrons with a reservoir, posing a significant challenge for molecular dynamics-based atomistic simulations that typically sample ensembles which conserve charge instead^{252,253}. Several approaches for including constant electrode potentials in MD simulations have been proposed^{254–257}, however this field is at a relatively early stage of development.

An important first step towards more realistic modelling of electrochemical systems is the ability to apply external electric fields in simulations. Electric fields may significantly influence catalytic activity, altering reaction pathways and energetics by modulating charge distributions and bonding character^{258,259}. Several distinct methods to incorporate electric fields in MLP-driven MD simulations have been reported^{260–265}. So far, applications of these methods have been limited to relatively simple systems such as liquid water^{263,265} and molecules in vacuum or solution^{260–262,264}. Taking advantage of these ML-accelerated methods to simulate catalytic reactions under electric fields over large time and length scales, particularly in complex heterogeneous environments, is an interesting area of research for the near future.

Nonadiabatic Effects and Multiple States MD simulations are most commonly performed under the Born-Oppenheimer approximation, which separates electronic and nuclear degrees of freedom due to their large difference in mass. In this framework, the electronic wavefunction is assumed to adapt instantaneously to changes in nuclear positions such that nuclei evolve on a single adiabatic PES. Nonadiabatic effects, which require a description beyond the Born-Oppenheimer approximation, play an important role in processes such as proton-coupled electron transfer reactions that govern many catalytic reactions^{266–268}, as well as in the dynamics of photoexcited charge carriers in photocatalysis^{269–271}. Accurate modelling of excited state dynamics often requires computationally expensive methods for the calculation of excited states, drastically limiting the accessible time and length scales that can be probed in simulations of nonadiabatic dynamics, for example using mixed quantum-classical dynamics approaches²⁷². Thus, machine learning acceleration for excited state dynamics could offer the same speed-up benefits that have revolutionized the field of ground-state molecular dynamics²⁷³.

Early work employed low-dimensional NNPs to represent constrained DFT (CDFT) spin states of O₂ on a frozen Al(111) slab^{121–123}, enabling investigation of nonadiabatic spin transitions through fewest-switches surface hopping simulations¹²⁴. More recently, several studies have demonstrated the potential of MLPs in excited state dynamics simulations by utilising machine-learned adiabatic excited states^{274–280}, or diabatic states from

CDFT²⁸¹. However, challenges remain due to the complexity of representing multiple excited states, especially if a large number of states is required, as well as difficulties in accurately reproducing the nonadiabatic coupling in strong-coupling regions where this quantity exhibits sharp peaks²⁷⁶.

We note that MLPs, as originally introduced, are designed to represent a single potential energy surface by constructing a structure-energy relationship. To represent multiple electronic states, one may either use individual MLPs for each state or employ extended architectures, such as models that predict multiple states simultaneously or encode each state as input to a single model²⁸². The ability to describe multiple states with MLPs is also critical in the context of magnetic materials, where the ground state magnetic order may change after the introduction of defects or dopants²⁸³, a topic of high interest in catalysis. Recently, adapted spin-dependent atom-centered symmetry functions have been proposed for this purpose²⁸³, as well as MPNN architectures that embed electronic structure information into their representation^{88,284}.

Nuclear Quantum Effects In addition to the Born-Oppenheimer approximation discussed above, a second approximation is often employed in MD simulations: the classical treatment of atomic nuclei as point particles which evolve in phase space according to Newton’s laws. Nuclear quantum effects (NQEs), such as zero-point energy and tunnelling, are particularly important at low temperature and in systems involving light elements, though they can significantly influence properties even at room temperature²⁸⁵. Path integral molecular dynamics, and related methods like ring polymer molecular dynamics, have emerged as efficient approaches to incorporate NQEs into atomistic simulations²⁸⁶. These methods involve sampling an extended classical phase space by representing each physical atom by a set of “beads”, typically around 10-100²⁸⁷. Calculations can be efficiently parallelized over beads, resulting in a computational overhead of only a factor of 10-100, far smaller than the gains achieved by replacing DFT with MLPs. Several studies have demonstrated the use of machine learning potentials to accelerate path-integral MD simulations^{236,285,288–306}. Of particular interest to heterogeneous catalysis is a recent study on proton hopping kinetics in zeolites²⁸⁵. NQEs, accounted for using MLP-accelerated ring polymer molecular dynamics, were found to drastically reduce activation energies for proton hopping and increase hopping rates. At 273 K, the proton hopping rate increased by a factor of 65, and even at 473 K it remained 7 times larger than in classical simulations. It can be anticipated that accounting for NQEs in atomistic simulations of catalytic systems will become considerably more common with the increasing prevalence of machine learning potentials.

V. CONCLUSIONS

The knowledge-based investigations of heterogeneous catalysis have traditionally been challenged by three well-known gaps: the complexity gap, the materials gap, and the pressure gap^{2,56}. One major example of the complexity gap that has slowed the theoretical modeling of heterogeneous catalysis is the gap between the time and length scales accessible with a quantum-mechanical treatment of atomic interactions and those required for realistic modeling of complex catalytic interfaces. Recently, Machine Learning Potentials have emerged as a powerful solution to bridge this *modeling gap*. Their ability to accurately learn reactive atomic interactions has allowed researchers to move beyond traditional tools and explore catalysis under more realistic conditions. With carefully constructed MLPs, simulations involving thousands of atoms over nanosecond timescales can now achieve quantum-mechanical accuracy, overcoming the limitations of conventional methods such as *ab initio* molecular dynamics and classical force fields.

In this article, we have explored the role of MLP-driven atomistic simulations in advancing our understanding of catalytic systems, including gas-phase and liquid-phase interfaces. Insights gained include elucidating reaction mechanisms, assessing solvent effects, and investigating the influence of defects and interfaces on catalytic processes. Furthermore, MLPs enable simulations under realistic *operando* conditions, capturing essential temperature effects and dynamic behaviors crucial for interpret-

ing catalytic activity in real-world applications. These results further highlight the potential of MLPs to advance our understanding of complex phenomena such as proton transfer, surface reconstructions, and nanoconfinement.

Despite their advantages, MLPs still require careful selection of training data, electronic structure methods, and validation of their transferability across various conditions. With the increasing availability of advanced yet user-friendly MLP packages, we expect the adoption of MLPs to become increasingly prevalent in heterogeneous catalysis research. Consequently, a shift from the traditional static view of catalytic systems to one that explicitly accounts for dynamic effects is expected. Such progress is likely to deepen our understanding of catalytic processes, ultimately guiding the design and optimization of new catalysts. Addressing current challenges, including improving data efficiency, capturing long-range interactions, and enhancing model robustness, is key to the further progress and broader adoption of MLPs in catalysis science.

ACKNOWLEDGMENTS

AO thanks the Deutsche Forschungsgemeinschaft (DFG) for funding in TRR/CRC 247 (A10, project number 388390466), JE thanks the DFG for funding in CRC 1633 (C04, project number 510228793), and KNL thanks the DFG for funding in CRC 1073 (C03, project number 217133147). Moreover, we are grateful for support by the DFG under Germany’s Excellence Strategy – EXC 2033 RESOLV (project-ID 390677874).

-
- ¹ Grünert, W.; Kleist, W.; Muhler, M. *Catalysis at surfaces*; Walter de Gruyter GmbH & Co KG, 2023.
 - ² Schlögl, R. Heterogeneous catalysis. *Angew. Chem. Int. Ed.* **2015**, *54*, 3465–3520.
 - ³ Fechete, I.; Wang, Y.; Védrine, J. C. The past, present and future of heterogeneous catalysis. *Catal. Today* **2012**, *189*, 2–27.
 - ⁴ Marcilly, C. Present status and future trends in catalysis for refining and petrochemicals. *J. Catal.* **2003**, *216*, 47–62.
 - ⁵ Humphreys, J.; Lan, R.; Tao, S. Development and recent progress on ammonia synthesis catalysts for Haber–Bosch process. *Adv. Energy Sustain. Res.* **2021**, *2*, 2000043.
 - ⁶ Cárdenas-Lizana, F.; Keane, M. A. The development of gold catalysts for use in hydrogenation reactions. *J. Mater. Sci.* **2013**, *48*, 543–564.
 - ⁷ Antolini, E. Catalysts for direct ethanol fuel cells. *J. Power Sources* **2007**, *170*, 1–12.
 - ⁸ Johnson, L. K.; Killian, C. M.; Brookhart, M. New Pd (II)- and Ni (II)-based catalysts for polymerization of ethylene and α -olefins. *J. Am. Chem. Soc.* **1995**, *117*, 6414–6415.
 - ⁹ Schlögl, R. Selective oxidation: from a still immature technology to the roots of catalysis science. *Top. Catal.* **2016**, *59*, 1461–1476.
 - ¹⁰ Najafshirtari, S.; Friedel Ortega, K.; Douthwaite, M.; Pattison, S.; Hutchings, G. J.; Bondue, C. J.; Tschulik, K.; Waffel, D.; Peng, B.; Deitermann, M., et al. A perspective on heterogeneous catalysts for the selective oxidation of alcohols. *Chem. Eur. J.* **2021**, *27*, 16809–16833.
 - ¹¹ Gewirth, A. A.; Niece, B. K. Electrochemical applications of in situ scanning probe microscopy. *Chem. Rev.* **1997**, *97*, 1129–1162.
 - ¹² Itaya, K. In situ scanning tunneling microscopy in electrolyte solutions. *Prog. Surf. Sci.* **1998**, *58*, 121–247.
 - ¹³ Shen, Y. R.; Ostroverkhov, V. Sum-frequency vibrational spectroscopy on water interfaces: polar orientation of water molecules at interfaces. *Chem. Rev.* **2006**, *106*, 1140–1154.
 - ¹⁴ Li, J.-F.; Zhang, Y.-J.; Ding, S.-Y.; Panneerselvam, R.; Tian, Z.-Q. Core-shell nanoparticle-enhanced Raman spectroscopy. *Chem. Rev.* **2017**, *117*, 5002–5069.
 - ¹⁵ Magnussen, O. M.; Groß, A. Toward an atomic-scale understanding of electrochemical interface structure and dynamics. *J. Am. Chem. Soc.* **2019**, *141*, 4777–4790.
 - ¹⁶ Nørskov, J. K.; Bligaard, T.; Rossmeisl, J.; Christensen, C. H. Towards the computational design of solid

- catalysts. *Nat. Chem.* **2009**, *1*, 37–46.
- 17 Rossmeisl, J.; Qu, Z.-W.; Zhu, H.; Kroes, G.-J.; Nørskov, J. K. Electrolysis of water on oxide surfaces. *Journal J. Electroanal. Chem.* **2007**, *607*, 83–89.
 - 18 Hussain, J.; Jónsson, H.; Skúlason, E. Faraday efficiency and mechanism of electrochemical surface reactions: CO₂ reduction and H₂ formation on Pt (111). *Faraday Discuss.* **2016**, *195*, 619–636.
 - 19 Skúlason, E.; Jonsson, H. Atomic scale simulations of heterogeneous electrocatalysis: recent advances. *Adv. Phys.: X* **2017**, *2*, 481–495.
 - 20 Nørskov, J. K.; Rossmeisl, J.; Logadottir, A.; Lindqvist, L.; Kitchin, J. R.; Bligaard, T.; Jónsson, H. Origin of the overpotential for oxygen reduction at a fuel-cell cathode. *J. Phys. Chem. B* **2004**, *108*, 17886–17892.
 - 21 Kulkarni, A.; Siahrostami, S.; Patel, A.; Nørskov, J. K. Understanding catalytic activity trends in the oxygen reduction reaction. *Chem. Rev.* **2018**, *118*, 2302–2312.
 - 22 Creazzo, F.; Galimberti, D. R.; Pezzotti, S.; Gaigeot, M.-P. DFT-MD of the (110)-Co₃O₄ cobalt oxide semiconductor in contact with liquid water, preliminary chemical and physical insights into the electrochemical environment. *J. Chem. Phys.* **2019**, *150*.
 - 23 Rahman, A.; Stillinger, F. H. Molecular dynamics study of liquid water. *J. Chem. Phys.* **1971**, *55*, 3336–3359.
 - 24 Barker, J.; Watts, R. Structure of water; A Monte Carlo calculation. *Chem. Phys. Lett.* **1969**, *3*, 144–145.
 - 25 Brooks, B. R.; Brooks III, C. L.; Mackerell Jr, A. D.; Nilsson, L.; Petrella, R. J.; Roux, B.; Won, Y.; Archontis, G.; Bartels, C.; Boresch, S., et al. CHARMM: the biomolecular simulation program. *J. Comput. Chem.* **2009**, *30*, 1545–1614.
 - 26 Case, D. A.; Darden, T. A.; Cheatham, T. E.; Simmerling, C. L.; Wang, J.; Duke, R. E.; Luo, R.; Crowley, M.; Walker, R. C.; Zhang, W., et al. Amber 10. **2008**,
 - 27 Senftle, T. P.; Hong, S.; Islam, M. M.; Kylasa, S. B.; Zheng, Y.; Shin, Y. K.; Junkermeier, C.; Engel-Herbert, R.; Janik, M. J.; Aktulga, H. M., et al. The ReaxFF reactive force-field: development, applications and future directions. *Npj Comput. Mater.* **2016**, *2*, 1–14.
 - 28 Daw, M. S.; Baskes, M. I. Embedded-atom method: Derivation and application to impurities, surfaces, and other defects in metals. *Phys. Rev. B* **1984**, *29*, 6443.
 - 29 Baskes, M. Application of the embedded-atom method to covalent materials: a semiempirical potential for silicon. *Phys. Rev. Lett* **1987**, *59*, 2666.
 - 30 Tersoff, J. New empirical approach for the structure and energy of covalent systems. *Phys. Rev. B* **1988**, *37*, 6991.
 - 31 Car, R.; Parrinello, M. Unified approach for molecular dynamics and density-functional theory. *Phys. Rev. Lett* **1985**, *55*, 2471.
 - 32 Marx, D.; Hutter, J. *Ab initio molecular dynamics: basic theory and advanced methods*; Cambridge University Press, 2009.
 - 33 Groß, A.; Sakong, S. Ab initio simulations of water/metal interfaces. *Chem. Rev.* **2022**, *122*, 10746–10776.
 - 34 Laio, A.; Parrinello, M. Escaping free-energy minima. *Proc. Natl. Acad. Sci. U.S.A.* **2002**, *99*, 12562–12566.
 - 35 Bussi, G.; Laio, A. Using metadynamics to explore complex free-energy landscapes. *Nat. Rev. Phys.* **2020**, *2*, 200–212.
 - 36 Torrie, G. M.; Valleau, J. P. Nonphysical sampling distributions in Monte Carlo free-energy estimation: Umbrella sampling. *J. Comput. Phys.* **1977**, *23*, 187–199.
 - 37 Behler, J. Representing potential energy surfaces by high-dimensional neural network potentials. *J. Phys. Condens. Matter* **2014**, *26*, 183001.
 - 38 Handley, C. M.; Popelier, P. L. A. Potential energy surfaces fitted by artificial neural networks. *J. Phys. Chem. A* **2010**, *114*, 3371–3383.
 - 39 Behler, J. Neural network potential-energy surfaces in chemistry: a tool for large-scale simulations. *Phys. Chem. Chem. Phys.* **2011**, *13*, 17930–17955.
 - 40 Behler, J. Perspective: machine learning potentials for atomistic simulations. *J. Chem. Phys.* **2016**, *145*, 170901.
 - 41 Unke, O. T.; Chmiela, S.; Sauceda, H. E.; Gastegger, M.; Poltavsky, I.; Schütt, K. T.; Tkatchenko, A.; Müller, K.-R. Machine Learning Force Fields. *Chem. Rev.* **2021**, *121*, 10142–10186.
 - 42 Friederich, P.; Häse, F.; Proppe, J.; Aspuru-Guzik, A. Machine-learned potentials for next-generation matter simulations. *Nat. Mater* **2021**, *20*, 750–761.
 - 43 Behler, J.; Csányi, G. Machine learning potentials for extended systems - a perspective. *Eur. Phys. J. B* **2021**, *94*, 142.
 - 44 Deringer, V. L.; Caro, M. A.; Csányi, G. Machine learning interatomic potentials as emerging tools for materials science. *Adv. Mater.* **2019**, *31*, 1902765.
 - 45 Eckhoff, M.; Behler, J. Insights into lithium manganese oxide–water interfaces using machine learning potentials. *J. Chem. Phys.* **2021**, *155*.
 - 46 Stukowski, A. Visualization and analysis of atomistic simulation data with OVITO-the Open Visualization Tool. *Modelling Simul. Mater. Sci. Eng.* **2010**, *18*.
 - 47 Blank, T. B.; Brown, S. D.; Calhoun, A. W.; Doren, D. J. Neural network models of potential energy surfaces. *J. Chem. Phys.* **1995**, *103*, 4129–4137.
 - 48 Chen, D.; Shang, C.; Liu, Z.-P. Machine-learning atomic simulation for heterogeneous catalysis. *Npj Comput. Mater.* **2023**, *9*, 2.
 - 49 Tang, D.; Ketkaew, R.; Luber, S. Machine learning interatomic potentials for heterogeneous catalysis. *Chem. Eur. J.* e202401148.
 - 50 Cheng, X.; Wu, C.; Xu, J.; Han, Y.; Xie, W.; Hu, P. Leveraging machine learning potentials for in-situ searching of active sites in heterogeneous catalysis. *Precis. Chem.* **2024**,
 - 51 Choung, S.; Park, W.; Moon, J.; Han, J. W. Rise of machine learning potentials in heterogeneous catalysis: Developments, applications, and prospects. *Chem. Eng. J.* **2024**, 152757.
 - 52 Zhou, Y.; Ouyang, Y.; Zhang, Y.; Li, Q.; Wang, J. Machine learning assisted simulations of electrochemical interfaces: recent progress and challenges. *J. Phys. Chem. Lett.* **2023**, *14*, 2308–2316.
 - 53 Hou, P.; Tian, Y.; Meng, X. Improving molecular dynamics simulations for solid-liquid interface with machine learning interatomic potentials. *Chem. Eur. J.* e202401373.
 - 54 Kitchin, J. R. Machine learning in catalysis. *Nat. Catal.* **2018**, *1*, 230–232.
 - 55 Ma, S.; Liu, Z.-P. Machine learning for atomic simulation and activity prediction in heterogeneous catalysis: current status and future. *ACS Catal.* **2020**, *10*, 13213–13226.
 - 56 Mou, T.; Pillai, H. S.; Wang, S.; Wan, M.; Han, X.; Schweitzer, N. M.; Che, F.; Xin, H. Bridging the com-

- plexity gap in computational heterogeneous catalysis with machine learning. *Nat. Catal.* **2023**, *6*, 122–136.
- ⁵⁷ Zhang, X.; Tian, Y.; Chen, L.; Hu, X.; Zhou, Z. Machine learning: a new paradigm in computational electrocatalysis. *J. Phys. Chem. Lett.* **2022**, *13*, 7920–7930.
- ⁵⁸ Chen, L.; Tian, Y.; Hu, X.; Yao, S.; Lu, Z.; Chen, S.; Zhang, X.; Zhou, Z. A universal machine learning framework for electrocatalyst innovation: a case study of discovering alloys for hydrogen evolution reaction. *Adv. Funct. Mater.* **2022**, *32*, 2208418.
- ⁵⁹ Margraf, J. T.; Jung, H.; Scheurer, C.; Reuter, K. Exploring catalytic reaction networks with machine learning. *Nat. Catal.* **2023**, *6*, 112–121.
- ⁶⁰ Dral, P. O. Quantum chemistry in the age of machine learning. *J. Phys. Chem. Lett.* **2020**, *11*, 2336–2347.
- ⁶¹ Noé, F.; Tkatchenko, A.; Müller, K.-R.; Clementi, C. Machine learning for molecular simulation. *Ann. Rev. Phys. Chem.* **2020**, *71*, 361–390.
- ⁶² Handley, C. M.; Behler, J. Next generation interatomic potentials for condensed systems. *Eur. Phys. J. B* **2014**, *87*, 152.
- ⁶³ Behler, J. Four generations of high-dimensional neural network potentials. *Chem. Rev.* **2021**, *121*, 10037–10072.
- ⁶⁴ Deringer, V. L.; Bartók, A. P.; Bernstein, N.; Wilkins, D. M.; Ceriotti, M.; Csányi, G. Gaussian process regression for materials and molecules. *Chem. Rev.* **2021**, *121*, 10073–10141.
- ⁶⁵ Kocer, E.; Ko, T. W.; Behler, J. Neural network potentials: A concise overview of methods. *Annu. Rev. Phys. Chem.* **2022**, *73*, 163–186.
- ⁶⁶ Ko, T. W.; Finkler, J. A.; Goedecker, S.; Behler, J. General-purpose machine learning potentials capturing nonlocal charge transfer. *Acc. Chem. Res.* **2021**, *54*, 808–817.
- ⁶⁷ Käser, S.; Vazquez-Salazar, L. I.; Meuwly, M.; Töpfer, K. Neural network potentials for chemistry: concepts, applications and prospects. *Digit. Discov.* **2023**, *2*, 28.
- ⁶⁸ Tokita, A. M.; Behler, J. Tutorial: How to Train a Neural Network Potential. *J. Chem. Phys.* **2023**, *159*, 121501.
- ⁶⁹ Behler, J.; Parrinello, M. Generalized neural-network representation of high-dimensional potential-energy surfaces. *Phys. Rev. Lett.* **2007**, *98*, 146401.
- ⁷⁰ Bartók, A. P.; Payne, M. C.; Kondor, R.; Csányi, G. Gaussian approximation potentials: the accuracy of quantum mechanics, without the electrons. *Phys. Rev. Lett.* **2010**, *104*, 136403.
- ⁷¹ Drautz, R. Atomic cluster expansion for accurate and transferable interatomic potentials. *Phys. Rev. B* **2019**, *99*, 014104.
- ⁷² Smith, J. S.; Isayev, O.; Roitberg, A. E. ANI-1: An extensible neural network potential with DFT accuracy at force field computational cost. *Chem. Sci.* **2017**, *8*, 3192–3203.
- ⁷³ Shapeev, A. V. Moment tensor potentials: A class of systematically improvable interatomic potentials. *Multiscale Model. Simul.* **2016**, *14*, 1153–1173.
- ⁷⁴ Zhang, L.; Han, J.; Wang, H.; Car, R.; E, W. Deep Potential Molecular Dynamics: A Scalable Model with the Accuracy of Quantum Mechanics. *Phys. Rev. Lett.* **2018**, *120*, 143001.
- ⁷⁵ Houlding, S.; Liem, S. Y.; Popelier, P. L. A. A polarizable high-rank quantum topological electrostatic potential developed using neural networks: Molecular dynamics simulations on the hydrogen fluoride dimer. *Int. J. Quantum Chem.* **2007**, *107*, 2817–2827.
- ⁷⁶ Artrith, N.; Morawietz, T.; Behler, J. High-dimensional neural-network potentials for multicomponent systems: Applications to zinc oxide. *Phys. Rev. B* **2011**, *83*, 153101.
- ⁷⁷ Morawietz, T.; Sharma, V.; Behler, J. A neural network potential-energy surface for the water dimer based on environment-dependent atomic energies and charges. *J. Chem. Phys.* **2012**, *136*, 064103.
- ⁷⁸ Unke, O. T.; Meuwly, M. PhysNet: A neural network for predicting energies, forces, dipole moments, and partial charges. *J. Chem. Theory Comput.* **2019**, *15*, 3678–3693.
- ⁷⁹ Yao, K.; Herr, J. E.; Toth, D. W.; Mckintyre, R.; Parkhill, J. The TensorMol-0.1 model chemistry: a neural network augmented with long-range physics. *Chem. Sci.* **2018**, *9*, 2261–2269.
- ⁸⁰ Bereau, T.; Andrienko, D.; von Lilienfeld, O. A. Transferable atomic multipole machine learning models for small organic molecules. *J. Chem. Theory Comput.* **2015**, *11*, 3225–3233.
- ⁸¹ Sifain, A. E.; Lubbers, N.; Nebgen, B. T.; Smith, J. S.; Lokhov, A. Y.; Isayev, O.; Roitberg, A. E.; Barros, K.; Tretyak, S. Discovering a transferable charge assignment model using machine learning. *J. Phys. Chem. Lett.* **2018**, *9*, 4495–4501.
- ⁸² Zhang, L.; Wang, H.; Muniz, M. C.; Panagiotopoulos, A. Z.; Car, R., et al. A deep potential model with long-range electrostatic interactions. *J. Chem. Phys.* **2022**, *156*.
- ⁸³ Gastegger, M.; Behler, J.; Marquetand, P. Machine learning molecular dynamics for the simulation of infrared spectra. *Chem. Sci.* **2017**, *8*, 6924–6935.
- ⁸⁴ Ghasemi, S. A.; Hofstetter, A.; Saha, S.; Goedecker, S. Interatomic potentials for ionic systems with density functional accuracy based on charge densities obtained by a neural network. *Phys. Rev. B* **2015**, *92*, 045131.
- ⁸⁵ Xie, X.; Persson, K. A.; Small, D. W. Incorporating electronic information into machine learning potential energy surfaces via approaching the ground-state electronic energy as a function of atom-based electronic populations. *J. Chem. Theory Comput.* **2020**, *16*, 4256–4270.
- ⁸⁶ Ko, T. W.; Finkler, J. A.; Goedecker, S.; Behler, J. A fourth-generation high-dimensional neural network potential with accurate electrostatics including non-local charge transfer. *Nat. Commun.* **2021**, *12*, 398.
- ⁸⁷ Khajepasha, E. R.; Finkler, J. A.; Kühne, T. D.; Ghasemi, S. A. CENT2: Improved charge equilibration via neural network technique. *Phys. Rev. B* **2022**, *105*, 144106.
- ⁸⁸ Unke, O. T.; Chmiela, S.; Gastegger, M.; Schütt, K. T.; Sauceda, H. E.; Müller, K.-R. SpookyNet: Learning force fields with electronic degrees of freedom and nonlocal effects. *Nat. Commun.* **2021**, *12*, 7273.
- ⁸⁹ Gilmer, J.; Schoenholz, S. S.; Riley, P. F.; Vinyals, O.; Dahl, G. E. Neural message passing for quantum chemistry. Proceedings of the 34th International Conference on Machine Learning. 2017; pp 1263–1272.
- ⁹⁰ Schütt, K. T.; Arbabzadah, F.; Chmiela, S.; Müller, K. R.; Tkatchenko, A. Quantum-chemical insights from deep tensor neural networks. *Nat. Commun.* **2017**, *8*, 13890.
- ⁹¹ Schütt, K. T.; Sauceda, H. E.; Kindermans, P.-J.; Tkatchenko, A.; Müller, K.-R. SchNet - A deep learning architecture for molecules and materials. *J. Chem. Phys.* **2018**, *148*, 241722.
- ⁹² Batzner, S.; Musaelian, A.; Sun, L.; Geiger, M.;

- Mailoa, J. P.; Kornbluth, M.; Molinari, N.; Smidt, T. E.; Kozinsky, B. E(3)-equivariant graph neural networks for data-efficient and accurate interatomic potentials. *Nat. Commun.* **2022**, *13*, 2453.
- ⁹³ Musaelian, A.; Batzner, S.; Johansson, A.; Sun, L.; Owen, C. J.; Kornbluth, M.; Kozinsky, B. Learning local equivariant representations for large-scale atomistic dynamics. *Nat. Commun.* **2023**, *14*, 579.
- ⁹⁴ Batatia, I.; Kovacs, D. P.; Simm, G.; Ortner, C.; Csanyi, G. MACE: Higher order equivariant message passing neural networks for fast and accurate force fields. *Adv. Neural Inf. Process. Syst.* 2022; pp 11423–11436.
- ⁹⁵ Ghosh Chaudhuri, R.; Paria, S. Core/shell nanoparticles: classes, properties, synthesis mechanisms, characterization, and applications. *Chem. Rev.* **2012**, *112*, 2373–2433.
- ⁹⁶ Artrith, N.; Behler, J. High-dimensional neural network potentials for metal surfaces: A prototype study for copper. *Phys. Rev. B* **2012**, *85*, 045439.
- ⁹⁷ Artrith, N.; Kolpak, A. M. Grand canonical molecular dynamics simulations of Cu–Au nanoalloys in thermal equilibrium using reactive ANN potentials. *Comp. Mater. Sci.* **2015**, *110*, 20–28.
- ⁹⁸ Weinreich, J.; Römer, A.; Paleico, M. L.; Behler, J. Properties of α -Brass nanoparticles. 1. Neural network potential energy surface. *J. Phys. Chem. C* **2020**, *124*, 12682–12695.
- ⁹⁹ Weinreich, J.; Paleico, M. L.; Behler, J. Properties of α -Brass Nanoparticles II: Structure and Composition. *J. Phys. Chem. C* **2021**, *125*, 14897.
- ¹⁰⁰ Liang, Y.; Mrovec, M.; Lysogorskiy, Y.; Vega-Paredes, M.; Scheu, C.; Drautz, R. Atomic cluster expansion for Pt–Rh catalysts: From ab initio to the simulation of nanoclusters in few steps. *Arxiv* **2023**,
- ¹⁰¹ Chiriki, S.; Jindal, S.; Bulusu, S. S. Neural network potentials for dynamics and thermodynamics of gold nanoparticles. *J. Chem. Phys.* **2017**, *146*, 084314.
- ¹⁰² Boes, J. R.; Groenenboom, M. C.; Keith, J. A.; Kitchin, J. R. Neural network and ReaxFF comparison for Au properties. *Int. J. Quantum Chem.* **2016**, *116*, 979–987.
- ¹⁰³ Loeffler, T. D.; Manna, S.; Patra, T. K.; Chan, H.; Narayanan, B.; Sankaranarayanan, S. Active learning a neural network model for gold clusters & bulk from sparse first principles training data. *ChemCatChem* **2020**, *12*, 4796–4806.
- ¹⁰⁴ Sun, G.; Sautet, P. Toward fast and reliable potential energy surfaces for metallic Pt clusters by hierarchical delta neural networks. *J. Chem. Theory Comput.* **2019**, *15*, 5614–5627.
- ¹⁰⁵ Chiriki, S.; Bulusu, S. S. Modeling of DFT quality neural network potential for sodium clusters: Application to melting of sodium clusters (Na₂₀ to Na₄₀). *Chem. Phys. Lett.* **2016**, *652*, 130–135.
- ¹⁰⁶ Gong, F.-Q.; Liu, Y.-P.; Wang, Y.; E, W.; Tian, Z.-Q.; Cheng, J. Machine learning molecular dynamics shows anomalous entropic effect on catalysis through surface pre-melting of nanoclusters. *Angew. Chem. Int. Ed.* **2024**, *63*, e202405379.
- ¹⁰⁷ Xu, J.; Xie, W.; Han, Y.; Hu, P. Atomistic insights into the oxidation of flat and stepped platinum surfaces using large-scale machine learning potential-based grand-canonical Monte Carlo. *ACS Catal.* **2022**, *12*, 14812–14824.
- ¹⁰⁸ Artrith, N.; Hiller, B.; Behler, J. Neural network potentials for metals and oxides: First applications to copper clusters at zinc oxide. *Phys. Status Solidi B* **2013**, *250*, 1191–1203.
- ¹⁰⁹ Paleico, M. L.; Behler, J. Global optimization of copper clusters at the ZnO(10 $\bar{1}$ 0) surface using a DFT-based neural network potential and genetic algorithms. *J. Chem. Phys.* **2020**, *153*, 054704.
- ¹¹⁰ Elias, J. S.; Artrith, N.; Bugnet, M.; Giordano, L.; Botton, G. A.; Kolpak, A. M.; Shao-Horn, Y. Elucidating the nature of the active phase in copper/ceria catalysts for CO oxidation. *ACS Catal.* **2016**, *6*, 1675–1679.
- ¹¹¹ Owen, C. J.; Marcella, N.; O’Connor, C. R.; Kim, T.-S.; Shimogawa, R.; Xie, C. Y.; Nuzzo, R. G.; Frenkel, A. I.; Reece, C.; Kozinsky, B. Surface roughening in nanoparticle catalysts. *arXiv preprint arXiv:2407.13643* **2024**,
- ¹¹² Wiesenekker, G.; Kroes, G. J.; Baerends, E. J. An analytical six-dimensional potential energy surface for dissociation of molecular hydrogen on Cu(100). *J. Chem. Phys.* **1996**, *104*, 7344.
- ¹¹³ Busnengo, H. F.; Salin, A.; Dong, W. Representation of the 6D potential energy surface for a diatomic molecule near a solid surface. *J. Chem. Phys.* **2000**, *112*, 7641.
- ¹¹⁴ Olsen, R. A.; Busnengo, H. F.; Salin, A.; Somers, M. F.; Kroes, G. J.; Baerends, E. J. Constructing accurate potential energy surfaces for a diatomic molecule interacting with a solid surface: H₂+Pt(111) and H₂+Cu(100). *J. Chem. Phys.* **2002**, *116*, 3841.
- ¹¹⁵ H.F. Busnengo, A., W. Dong Six-dimensional classical dynamics of H₂ dissociative adsorption on Pd(111). *Chem. Phys. Lett.* **2000**, *320*, 328.
- ¹¹⁶ Crespos, C.; Collins, M. A.; Pijper, E.; Kroes, G. J. Multi-dimensional potential energy surface determination by modified Shepard interpolation for a molecule-surface reaction: H₂+Pt(111). *Chem. Phys. Lett.* **2003**, *376*, 566–575.
- ¹¹⁷ Daz, C.; Olsen, R. A.; Busnengo, H. F.; Kroes, G. J. Dynamics on six-Dimensional potential energy surfaces for H₂/Cu(111): corrugation reducing procedure versus modified shepard interpolation method and PW91 versus RPBE. *J. Phys. Chem. C* **2010**, *114*, 11192.
- ¹¹⁸ Lorenz, S.; Groß, A.; Scheffler, M. Representing high-dimensional potential-energy surfaces for reactions at surfaces by neural networks. *Chem. Phys. Lett.* **2004**, *395*, 210–215.
- ¹¹⁹ Lorenz, S.; Scheffler, M.; Groß, A. Descriptions of surface chemical reactions using a neural network representation of the potential energy surface. *Phys. Rev. B* **2006**, *73*, 115431.
- ¹²⁰ Behler, J.; Delley, B.; Lorenz, S.; Reuter, K.; Scheffler, M. Dissociation of O₂ at Al(111): the role of spin selection rules. *Phys. Rev. Lett.* **2005**, *94*, 36104.
- ¹²¹ Behler, J.; Lorenz, S.; Reuter, K. Representing molecule-surface interactions with symmetry-adapted neural networks. *J. Chem. Phys.* **2007**, *127*, 014705.
- ¹²² Behler, J.; Reuter, K.; Scheffler, M. Nonadiabatic effects in the dissociation of oxygen molecules at the Al(111) surface. *Phys. Rev. B* **2008**, *77*, 115421.
- ¹²³ Carbogno, C.; Behler, J.; Groß, A.; Reuter, K. Fingerprints for spin-selection rules in the interaction dynamics of O₂ at Al(111). *Phys. Rev. Lett.* **2008**, *101*, 096104.
- ¹²⁴ Carbogno, C.; Behler, J.; Reuter, K.; Groß, A. Signatures of nonadiabatic O₂ dissociation at Al(111): First-principles fewest-switches study. *Phys. Rev. B* **2010**, *81*, 035410.

- ¹²⁵ Goikoetxea, I.; Beltrán, J.; Meyer, J.; Juaristi, J. I.; Alducin, M.; Reuter, K. Non-adiabatic effects during the dissociative adsorption of O₂ at Ag(111)? A first-principles divide and conquer study. *New J. Phys.* **2012**, *14*, 013050.
- ¹²⁶ Goikoetxea, I.; Meyer, J.; Juaristi, J. I.; Alducin, M.; Reuter, K. Role of physisorption states in molecular scattering: A semilocal density-functional theory study on O₂ Ag(111). *Phys. Rev. Lett.* **2014**, *112*, 156101.
- ¹²⁷ Bonati, L.; Polino, D.; Pizzolitto, C.; Biasi, P.; Eckert, R.; Reitmeier, S.; Schlögl, R.; Parrinello, M. The role of dynamics in heterogeneous catalysis: Surface diffusivity and N₂ decomposition on Fe (111). *Proc. Natl. Acad. Sci. U.S.A.* **2023**, *120*, e2313023120.
- ¹²⁸ Purcel, M.; Berendts, S.; Bonati, L.; Perego, S.; Müller, A.; Lerch, M.; Parrinello, M.; Muhler, M. Iron nitride formation and decomposition during ammonia decomposition over a wustite-based bulk iron catalyst. *ACS Catal.* **2024**, *14*, 13947–13957.
- ¹²⁹ Perego, S.; Bonati, L.; Tripathi, S.; Parrinello, M. How dynamics changes ammonia cracking on iron surfaces. *ACS Catal.* **2024**, *14*, 14652–14664.
- ¹³⁰ Tripathi, S.; Bonati, L.; Perego, S.; Parrinello, M. How poisoning is avoided in a step of relevance to the Haber–Bosch catalysis. *ACS Catal.* **2024**, *14*, 4944–4950.
- ¹³¹ Chame, A.; Lançon, F.; Politi, P.; Renaud, G.; Vilfan, I.; Villain, J. Three mysteries in surface science. *Int. J. Mod. Phys. B* **1997**, *11*.
- ¹³² Hütner, J. I.; Conti, A.; Kugler, D.; Mittendorfer, F.; Kresse, G.; Schmid, M.; Diebold, U.; Balajka, J. Stoichiometric reconstruction of the Al₂O₃ (0001) surface. *Science* **2024**, *385*, 1241–1244.
- ¹³³ Jinnouchi, R.; Karsai, F.; Kresse, G. On-the-fly machine learning force field generation: Application to melting points. *Phys. Rev. B* **2019**, *100*, 014105.
- ¹³⁴ Jinnouchi, R.; Lahnsteiner, J.; Karsai, F.; Kresse, G.; Bokdam, M. Phase transitions of hybrid perovskites simulated by machine-learning force fields trained on the fly with Bayesian inference. *Phys. Rev. Lett.* **2019**, *122*, 225701.
- ¹³⁵ Jinnouchi, R.; Karsai, F.; Verdi, C.; Asahi, R.; Kresse, G. Descriptors representing two- and three-body atomic distributions and their effects on the accuracy of machine-learned inter-atomic potentials. *J. Chem. Phys.* **2020**, *152*.
- ¹³⁶ Liebetau, M.; Dorenkamp, Y.; Bünermann, O.; Behler, J. Hydrogen atom scattering at the Al₂O₃(0001) surface: a combined experimental and theoretical study. *Phys. Chem. Chem. Phys.* **2024**, *26*, 1696.
- ¹³⁷ Ludwig, J.; Vlachos, D. G. Ab initio molecular dynamics of hydrogen dissociation on metal surfaces using neural networks and novelty sampling. *J. Chem. Phys.* **2007**, *127*, 154716.
- ¹³⁸ Sumaria, V.; Nguyen, L.; Tao, F. F.; Sautet, P. Atomic-scale mechanism of platinum catalyst restructuring under a pressure of reactant gas. *J. Am. Chem. Soc.* **2022**, *145*, 392–401.
- ¹³⁹ Vandermause, J.; Xie, Y.; Lim, J. S.; Owen, C. J.; Kozinsky, B. Active learning of reactive Bayesian force fields applied to heterogeneous catalysis dynamics of H/Pt. *Nat. Commun.* **2022**, *13*, 5183.
- ¹⁴⁰ Gerrits, N. Accurate simulations of the reaction of H₂ on a curved Pt crystal through machine learning. *J. Phys. Chem. Lett.* **2021**, *12*, 12157–12164.
- ¹⁴¹ Manzhos, S.; Yamashita, K. A model for the dissociative adsorption of N₂O on Cu(100) using a continuous potential energy surface. *Surf. Sci.* **2010**, *604*, 554–560.
- ¹⁴² Meyer, J.; Reuter, K. Modeling heat dissipation at the nanoscale: An embedding approach for chemical reaction dynamics on metal surfaces. *Angew. Chem. Int. Ed.* **2014**, *53*, 4721–4724.
- ¹⁴³ Füchsel, G.; del Cueto, M.; Diaz, C.; Kroes, G.-J. Enigmatic HCl + Au(111) reaction: a puzzle for theory and experiment. *J. Phys. Chem. C* **2016**, *120*, 25760–25779.
- ¹⁴⁴ Zhou, X.; Nattino, F.; Zhang, Y.; Chen, J.; Kroes, G.-J.; Guo, H.; Jiang, B. Dissociative chemisorption of methane on Ni(111) using a chemically accurate fifteen dimensional potential energy surface. *Phys. Chem. Chem. Phys.* **2017**, *19*, 30540–30550.
- ¹⁴⁵ Xu, Y.; Jin, Y.; García Sánchez, J. S.; Pérez-Lemus, G. R.; Zubieta Rico, P. F.; Delferro, M.; de Pablo, J. J. A Molecular View of Methane Activation on Ni (111) through Enhanced Sampling and Machine Learning. *J. Phys. Chem. Lett.* **2024**, *15*, 9852–9862.
- ¹⁴⁶ Shakouri, K.; Behler, J.; Meyer, J.; Kroes, G.-J. Accurate neural network description of surface phonons in reactive gas-surface dynamics: N₂+Ru(0001). *J. Phys. Chem. Lett.* **2017**, *8*, 2131–2136.
- ¹⁴⁷ Shakouri, K.; Behler, J.; Meyer, J.; Kroes, G.-J. Analysis of energy dissipation channels in a benchmark system of activated dissociation: N₂ on Ru(0001). *J. Phys. Chem. C* **2018**, *122*, 23470–23480.
- ¹⁴⁸ Gerrits, N.; Shakouri, K.; Behler, J.; Kroes, G.-J. Accurate probabilities for highly activated reaction of polyatomic molecules on surfaces using a high-dimensional neural network potential: CHD₃ + Cu(111). *J. Phys. Chem. Lett.* **2019**, *10*, 1763–1768.
- ¹⁴⁹ Spiering, P.; Shakouri, K.; Behler, J.; Kroes, G.-J.; Meyer, J. Orbital-dependent electronic friction significantly affects the description of reactive scattering of N₂ from Ru(0001). *J. Phys. Chem. Lett.* **2019**, *10*, 2957–2962.
- ¹⁵⁰ Wille, S.; Jiang, H.; Bünermann, O.; Wodtke, A. M.; Behler, J.; Kandratsenka, A. An experimentally validated neural-network potential energy surface for H atoms on free-standing graphene in full dimensionality. *Phys. Chem. Chem. Phys.* **2020**, *22*, 26113–26120.
- ¹⁵¹ Boes, J. R.; Kitchin, J. R. Neural network predictions of oxygen interactions on a dynamic Pd surface. *Modell. Simul.* **2017**, *43*, 346–354.
- ¹⁵² Stark, W. G.; van der Oord, C.; Batatia, I.; Zhang, Y.; Jiang, B.; Csányi, G.; Maurer, R. J. Benchmarking of machine learning interatomic potentials for reactive hydrogen dynamics at metal surfaces. *arXiv preprint arXiv:2403.15334* **2024**,
- ¹⁵³ Stark, W. G.; Westermayr, J.; Douglas-Gallardo, O. A.; Gardner, J.; Habershon, S.; Maurer, R. J. Importance of equivariant features in machine-learning interatomic potentials for reactive chemistry at metal surfaces. *Arxiv* **2023**,
- ¹⁵⁴ Žugec, I.; Tetenoire, A.; Muzas, A. S.; Zhang, Y.; Jiang, B.; Alducin, M.; Juaristi, J. I. Understanding the photoinduced desorption and oxidation of CO on Ru (0001) using a neural network potential energy surface. *JACS Au* **2024**,
- ¹⁵⁵ Perego, S.; Bonati, L. Data-efficient modeling of catalytic reactions via enhanced sampling and on-the-fly learning of machine learning potentials. 2024.
- ¹⁵⁶ Artrith, N.; Kolpak, A. M. Understanding the composi-

- tion and activity of electrocatalytic nanoalloys in aqueous solvents: a combination of DFT and accurate neural network potentials. *Nano Lett.* **2014**, *14*, 2670–2676.
- ¹⁵⁷ Natarajan, S. K.; Behler, J. Neural network molecular dynamics simulations of solid–liquid interfaces: water at low-index copper surfaces. *Phys. Chem. Chem. Phys.* **2016**, *18*, 28704–28725.
- ¹⁵⁸ Quaranta, V.; Hellström, M.; Behler, J. Proton-transfer mechanisms at the water–ZnO interface: The role of pre-solvation. *J. Phys. Chem. Lett.* **2017**, *8*, 1476–1483.
- ¹⁵⁹ Quaranta, V.; Hellström, M.; Behler, J.; Kullgren, J.; Mitev, P. D.; Hermansson, K. Maximally resolved anharmonic OH vibrational spectrum of the water/ZnO (101⁻0) interface from a high-dimensional neural network potential. *J. Chem. Phys.* **2018**, *148*.
- ¹⁶⁰ Quaranta, V.; Behler, J.; Hellström, M. Structure and dynamics of the liquid–water/zinc-oxide interface from machine learning potential simulations. *J. Phys. Chem. C* **2018**, *123*, 1293–1304.
- ¹⁶¹ Hellström, M.; Quaranta, V.; Behler, J. One-dimensional vs. two-dimensional proton transport processes at solid–liquid zinc-oxide–water interfaces. *Chem. Sci.* **2019**, *10*, 1232–1243.
- ¹⁶² Kobayashi, T.; Ikeda, T.; Nakayama, A. Long-range proton and hydroxide ion transfer dynamics at the water/CeO₂ interface in the nanosecond regime: reactive molecular dynamics simulations and kinetic analysis. *Chem. Sci.* **2024**, *15*, 6816–6832.
- ¹⁶³ Andrade, M. F. C.; Ko, H.-Y.; Zhang, L.; Car, R.; Selloni, A. Free energy of proton transfer at the water–TiO₂ interface from ab initio deep potential molecular dynamics. *Chem. Sci.* **2020**, *11*, 2335–2341.
- ¹⁶⁴ Schran, C.; Thiemann, F. L.; Rowe, P.; Müller, E. A.; Marsalek, O.; Michaelides, A. Machine learning potentials for complex aqueous systems made simple. *Proc. Natl. Acad. Sci. U.S.A.* **2021**, *118*, e2110077118.
- ¹⁶⁵ O’Connor, C. R.; Calegari Andrade, M. F.; Selloni, A.; Kimmel, G. A. Elucidating the water–anatase TiO₂(101) interface structure using infrared signatures and molecular dynamics. *J. Chem. Phys.* **2023**, *159*.
- ¹⁶⁶ Li, Z.; Wang, J.; Yang, C.; Liu, L.; Yang, J.-Y. Thermal transport across TiO₂–H₂O interface involving water dissociation: Ab initio-assisted deep potential molecular dynamics. *J. Chem. Phys.* **2023**, *159*.
- ¹⁶⁷ Zhuang, Y.-B.; Bi, R.-H.; Cheng, J. Resolving the odd–even oscillation of water dissociation at rutile TiO₂(110)–water interface by machine learning accelerated molecular dynamics. *J. Chem. Phys.* **2022**, *157*.
- ¹⁶⁸ Wen, B.; Calegari Andrade, M. F.; Liu, L.-M.; Selloni, A. Water dissociation at the water–rutile TiO₂(110) interface from ab initio-based deep neural network simulations. *Proc. Natl. Acad. Sci. U.S.A.* **2023**, *120*, e2212250120.
- ¹⁶⁹ Zeng, Z.; Wodaczek, F.; Liu, K.; Stein, F.; Hutter, J.; Chen, J.; Cheng, B. Mechanistic insight on water dissociation on pristine low-index TiO₂ surfaces from machine learning molecular dynamics simulations. *Nat. Commun.* **2023**, *14*, 6131.
- ¹⁷⁰ Schneider, J.; Matsuoaka, M.; Takeuchi, M.; Zhang, J.; Horiuchi, Y.; Anpo, M.; Bahnemann, D. W. Understanding TiO₂ photocatalysis: mechanisms and materials. *Chem. Rev.* **2014**, *114*, 9919–9986.
- ¹⁷¹ Selloni, A. Aqueous Titania Interfaces. *Annu. Rev. Phys. Chem.* **2024**, *75*.
- ¹⁷² Li, Z.; Tan, X.; Fu, Z.; Liu, L.; Yang, J.-Y. Thermal transport across copper–water interfaces according to deep potential molecular dynamics. *Phys. Chem. Chem. Phys.* **2023**, *25*, 6746–6756.
- ¹⁷³ Harris, L. A.; Quong, A. A. Molecular chemisorption as the theoretically preferred pathway for water adsorption on ideal rutile TiO₂. *Phys. Rev. Lett.* **2004**, *93*, 086105.
- ¹⁷⁴ Li, L.; Calegari Andrade, M. F.; Car, R.; Selloni, A.; Carter, E. A. Characterizing structure-dependent TiS₂/water interfaces using deep-neural-network-assisted molecular dynamics. *J. Phys. Chem. C* **2023**, *127*, 9750–9758.
- ¹⁷⁵ Cady, C. W.; Gardner, G.; Maron, Z. O.; Retuerto, M.; Go, Y. B.; Segan, S.; Greenblatt, M.; Dismukes, G. C. Tuning the Electrocatalytic Water Oxidation Properties of AB₂O₄ Spinel Nanocrystals: A (Li, Mg, Zn) and B (Mn, Co) Site Variants of LiMn₂O₄. *ACS Catal.* **2015**, *5*, 3403–3410.
- ¹⁷⁶ Schienbein, P.; Blumberger, J. Nanosecond solvation dynamics of the hematite/liquid water interface at hybrid DFT accuracy using committee neural network potentials. *Phys. Chem. Chem. Phys.* **2022**, *24*, 15365–15375.
- ¹⁷⁷ Fan, X.-T.; Wen, X.-J.; Zhuang, Y.-B.; Cheng, J. Molecular insight into the GaP (110)–water interface using machine learning accelerated molecular dynamics. *J. Energy Chem.* **2023**, *82*, 239–247.
- ¹⁷⁸ Piaggi, P. M.; Selloni, A.; Panagiotopoulos, A. Z.; Car, R.; Debenedetti, P. G. A first-principles machine-learning force field for heterogeneous ice nucleation on microcline feldspar. *Faraday Discuss.* **2024**, *249*, 98–113.
- ¹⁷⁹ Raman, A. S.; Selloni, A. An ab-initio deep neural network potential for accurate large-scale simulations of the muscovite mica-water interface. *Mol. Phys.* **2024**, e2365430.
- ¹⁸⁰ Raman, A. S.; Selloni, A. Insights into the structure and dynamics of K⁺ ions at the muscovite–water interface from machine learning potential simulations. *J. Chem. Phys.* **2024**, *160*.
- ¹⁸¹ Zhang, L.; Chen, M.; Wu, X.; Wang, H.; E, W.; Car, R. Deep neural network for the dielectric response of insulators. *Phys. Rev. B* **2020**, *102*, 041121.
- ¹⁸² Sommers, G. M.; Andrade, M. F. C.; Zhang, L.; Wang, H.; Car, R. Raman spectrum and polarizability of liquid water from deep neural networks. *Phys. Chem. Chem. Phys.* **2020**, *22*, 10592–10602.
- ¹⁸³ Du, X.; Shao, W.; Bao, C.; Zhang, L.; Cheng, J.; Tang, F. Revealing the molecular structures of α -Al₂O₃ (0001)–water interface by machine learning based computational vibrational spectroscopy. *J. Chem. Phys.* **2024**, *161*.
- ¹⁸⁴ Raman, A. S.; Selloni, A. Acid–base chemistry of a model iro₂ catalytic interface. *J. Phys. Chem. Lett.* **2023**, *14*, 7787–7794.
- ¹⁸⁵ Jia, M.; Zhuang, Y.-B.; Wang, F.; Zhang, C.; Cheng, J. Water-mediated proton hopping mechanisms at the SnO₂ (110)/H₂O interface from ab initio deep potential molecular dynamics. *Precis. Chem.* **2024**,
- ¹⁸⁶ Wang, F.; Cheng, J. Automated workflow for computation of redox potentials, acidity constants, and solvation free energies accelerated by machine learning. *J. Chem. Phys.* **2022**, *157*.
- ¹⁸⁷ Wang, F.; Ma, Z.; Cheng, J. Accelerating computation of acidity constants and redox potentials for aqueous organic redox flow batteries by machine learning potential-based molecular dynamics. *J. Am. Chem. Soc.* **2024**, *146*, 14566–14575.

- 188 Schienbein, P.; Blumberger, J. Data-efficient active learning for thermodynamic integration: acidity constants of BiVO_4 in water. *ChemPhysChem* e202400490.
- 189 Mikkelsen, A. E.; Schiøtz, J.; Vegge, T.; Jacobsen, K. W. Is the water/Pt (111) interface ordered at room temperature? *J. Chem. Phys.* **2021**, *155*.
- 190 Mikkelsen, A. E.; Kristoffersen, H. H.; Schiøtz, J.; Vegge, T.; Hansen, H. A.; Jacobsen, K. W. Structure and energetics of liquid water-hydroxyl layers on Pt (111). *Phys. Chem. Chem. Phys.* **2022**, *24*, 9885–9890.
- 191 Wang, F.-T.; Liu, X.; Cheng, J. Water structures and anisotropic dynamics at Pt(211)/water interface revealed by machine learning molecular dynamics. *Mater. Futures* **2024**, *3*, 041001.
- 192 Gäding, J.; Della Balda, V.; Lan, J.; Konrad, J.; Iannuzzi, M.; Meißner, R.; Tocci, G. The role of the water contact layer on hydration and transport at solid/liquid interfaces. *Proc. Natl. Acad. Sci. U.S.A.* **2024**, *121*, e2407877121.
- 193 Sun, Y.; Wu, C.-R.; Wang, F.; Bi, R.-H.; Zhuang, Y.-B.; Liu, S.; Chen, M.-S.; Zhang, K. H.-L.; Yan, J.-W.; Mao, B.-W., et al. Step-induced double-row pattern of interfacial water on rutile TiO_2 (110) under electrochemical conditions. *Chem. Sci.* **2024**, *15*, 12264–12269.
- 194 Kondati Natarajan, S.; Behler, J. Self-diffusion of surface defects at copper–water interfaces. *J. Phys. Chem. C* **2017**, *121*, 4368–4383.
- 195 Li, X.; Paier, W.; Paier, J. Machine learning in computational surface science and catalysis: Case studies on water and metal–oxide interfaces. *Front. Chem.* **2020**, *8*, 601029.
- 196 Nakanishi, A.; Kasamatsu, S.; Haruyama, J.; Sugino, O. Structural analysis of zirconium oxynitride/water interface using neural network potential. *arXiv preprint arXiv:2307.11296* **2023**,
- 197 Goldsmith, B. R.; Peters, B.; Johnson, J. K.; Gates, B. C.; Scott, S. L. Beyond ordered materials: understanding catalytic sites on amorphous solids. *ACS Catal.* **2017**, *7*, 7543–7557.
- 198 Ding, Z.; Selloni, A. Modeling the aqueous interface of amorphous TiO_2 using deep potential molecular dynamics. *J. Chem. Phys.* **2023**, *159*.
- 199 Calegari Andrade, M. F.; Ko, H.-Y.; Car, R.; Selloni, A. Structure, polarization, and sum frequency generation spectrum of interfacial water on anatase TiO_2 . *J. Phys. Chem. Lett.* **2018**, *9*, 6716–6721.
- 200 Li, Z.; Hu, Z.; Wang, Y.; Ouyang, R. Molecular dynamics simulation of Co–Fe-based perovskite oxide/water interfaces. *J. Phys. Chem. C* **2024**,
- 201 Bliem, R.; McDermott, E.; Ferstl, P.; Setvin, M.; Gamba, O.; Pavelec, J.; Schneider, M.; Schmid, M.; Diebold, U.; Blaha, P., et al. Subsurface cation vacancy stabilization of the magnetite (001) surface. *Science* **2014**, *346*, 1215–1218.
- 202 Romano, S.; de Hijes, P. M.; Meier, M.; Kresse, G.; Franchini, C.; Dellago, C. Structure and dynamics of the magnetite (001)/water interface from molecular dynamics simulations based on a neural network potential. *arXiv preprint arXiv:2408.11538* **2024**,
- 203 Wordsworth, J.; Benedetti, T. M.; Somerville, S. V.; Schuhmann, W.; Tilley, R. D.; Gooding, J. J. The influence of nanoconfinement on electrocatalysis. *Angew. Chem. Int. Ed.* **2022**, *61*, e202200755.
- 204 Ghorbanfekr, H.; Behler, J.; Peeters, F. M. Insights into water permeation through hBN nanocapillaries by ab initio machine learning molecular dynamics simulations. *J. Phys. Chem. Lett.* **2020**, *11*, 7363–7370.
- 205 Zhao, W.; Qiu, H.; Guo, W. A deep neural network potential for water confined in graphene nanocapillaries. *J. Phys. Chem. C* **2022**, *126*, 10546–10553.
- 206 Liu, D.; Wu, J.; Lu, D. Transferability evaluation of the deep potential model for simulating water-graphene confined system. *J. Chem. Phys.* **2023**, *159*.
- 207 Secchi, E.; Marbach, S.; Niguès, A.; Stein, D.; Siria, A.; Bocquet, L. Massive radius-dependent flow slippage in carbon nanotubes. *Nature* **2016**, *537*, 210–213.
- 208 Thiemann, F. L.; Schran, C.; Rowe, P.; Müller, E. A.; Michaelides, A. Water flow in single-wall nanotubes: Oxygen makes it slip, hydrogen makes it stick. *ACS Nano* **2022**, *16*, 10775–10782.
- 209 Kwon, H.; Calegari Andrade, M. F.; Ardo, S.; Esposito, D. V.; Pham, T. A.; Ogitsu, T. Confinement effects on proton transfer in TiO_2 nanopores from machine learning potential molecular dynamics simulations. *ACS Appl. Mater. Interfaces.* **2024**,
- 210 Chen, B. W.; Zhang, X.; Zhang, J. Accelerating explicit solvent models of heterogeneous catalysts with machine learning interatomic potentials. *Chem. Sci.* **2023**, *14*, 8338–8354.
- 211 Yang, X.; Bhowmik, A.; Vegge, T.; Hansen, H. A. Neural network potentials for accelerated metadynamics of oxygen reduction kinetics at Au–water interfaces. *Chem. Sci.* **2023**, *14*, 3913–3922.
- 212 Schütt, K.; Unke, O.; Gastegger, M. Equivariant message passing for the prediction of tensorial properties and molecular spectra. *Int. Conf. Mach. Learn.* 2021; pp 9377–9388.
- 213 Kuang, P.; Low, J.; Cheng, B.; Yu, J.; Fan, J. MXene-based photocatalysts. *J. Mater. Sci. Technol.* **2020**, *56*, 18–44.
- 214 Hou, P.; Tian, Y.; Xie, Y.; Li, Q.; Chen, G.; Du, F.; Wu, J.; Ma, Y.; Meng, X. Proton-driven dynamic behavior of nanoconfined water in hydrophilic MXene sheets. *Angew. Chem. Int. Ed.* e202411849.
- 215 Hou, P.; Tian, Y.; Xie, Y.; Du, F.; Chen, G.; Vojvodic, A.; Wu, J.; Meng, X. Unraveling the oxidation behaviors of MXenes in aqueous systems by active-learning-potential molecular-dynamics simulation. *Angew. Chem.* **2023**, *135*, e202304205.
- 216 Raman, A. S.; Selloni, A. Long timescale molecular dynamics simulations of carboxylic acid-modified anatase TiO_2 (101)-water interfaces using ab-initio deep neural network potentials. *Surf. Sci.* **2024**, 122595.
- 217 Zhang, C.; Andrade, M. C.; Goldsmith, Z. K.; Raman, A. S.; Li, Y.; Piaggi, P.; Wu, X.; Car, R.; Selloni, A. Electrical double layer and capacitance of TiO_2 electrolyte interfaces from first principles simulations. *arXiv preprint arXiv:2404.00167* **2024**,
- 218 Bard, A. J.; Faulkner, L. R.; White, H. S. *Electrochemical methods: fundamentals and applications*; John Wiley & Sons, 2022.
- 219 Be, Y.; De Bruyn, P., et al. Adsorption at the rutile-solution interface: II. Model of the electrochemical double layer. *J. Colloid Interface Sci.* **1968**, *28*, 92–105.
- 220 Zare, M.; Sahas, D.; Saleheen, M.; Behler, J.; Heyden, A. Hybrid quantum mechanical, molecular mechanical, and machine learning potential for computing aqueous-phase adsorption free energies on metal surfaces. *J. Chem. The-*

- ory Comput. **2024**,
- ²²¹ Schran, C.; Brezina, K.; Marsalek, O. Committee neural network potentials control generalization errors and enable active learning. *J. Chem. Phys.* **2020**, *153*.
- ²²² Seung, H. S.; Oppen, M.; Sompolinsky, H. Query by committee. Proc. Annu. Workshop Comput. Learn. Theory. 1992; pp 287–294.
- ²²³ Krogh, A.; Vedelsby, J. Neural network ensembles, cross validation, and active learning. *Adv. Neural Inf. Process. Syst.* **1994**, *7*.
- ²²⁴ Smith, J. S.; Nebgen, B.; Lubbers, N.; Isayev, O.; Roitberg, A. E. Less is more: Sampling chemical space with active learning. *J. Chem. Phys.* **2018**, *148*.
- ²²⁵ Yang, M.; Bonati, L.; Polino, D.; Parrinello, M. Using metadynamics to build neural network potentials for reactive events: the case of urea decomposition in water. *Catal. Today* **2022**, *387*, 143–149.
- ²²⁶ Jung, H.; Covino, R.; Arjun, A.; Leitold, C.; Dellago, C.; Bolhuis, P. G.; Hummer, G. Machine-guided path sampling to discover mechanisms of molecular self-organization. *Nat. Comput. Sci.* **2023**, *3*, 334–345.
- ²²⁷ Zou, Z.; Beyerle, E. R.; Tsai, S.-T.; Tiwary, P. Driving and characterizing nucleation of urea and glycine polymorphs in water. *Proc. Natl. Acad. Sci. U.S.A.* **2023**, *120*, e2216099120.
- ²²⁸ Batzner, S.; Musaelian, A.; Kozinsky, B. Advancing molecular simulation with equivariant interatomic potentials. *Nat. Rev. Phys.* **2023**, *5*, 437–438.
- ²²⁹ Thomas, N.; Smidt, T.; Kearnes, S.; Yang, L.; Li, L.; Kohlhoff, K.; Riley, P. Tensor field networks: Rotation- and translation-equivariant neural networks for 3d point clouds. *arXiv preprint arXiv:1802.08219* **2018**,
- ²³⁰ Weiler, M.; Geiger, M.; Welling, M.; Boomsma, W.; Cohen, T. S. 3d steerable cnns: Learning rotationally equivariant features in volumetric data. *Adv. Neural Inf. Process. Syst.* **2018**, *31*.
- ²³¹ Batatia, I.; Benner, P.; Chiang, Y.; Elena, A. M.; Kovács, D. P.; Riebesell, J.; Advincula, X. R.; Asta, M.; Baldwin, W. J.; Bernstein, N., et al. A foundation model for atomistic materials chemistry. *arXiv preprint arXiv:2401.00096* **2023**,
- ²³² Falk, J.; Bonati, L.; Novelli, P.; Parrinello, M.; Pontil, M. Transfer learning for atomistic simulations using GNNs and kernel mean embeddings. *Adv. Neural Inf. Process. Syst.* **2024**, *36*.
- ²³³ Morawietz, T.; Singraber, A.; Dellago, C.; Behler, J. How van der Waals interactions determine the unique properties of water. *Proc. Natl. Acad. Sci.* **2016**, *113*, 8368–8373.
- ²³⁴ Yu, Q.; Qu, C.; Houston, P. L.; Conte, R.; Nandi, A.; Bowman, J. M. q-AQUA: A many-body CCSD(T) water potential, including four-body interactions, demonstrates the quantum nature of water from clusters to the liquid phase. *J. Phys. Chem. Lett.* **2022**, *13*, 5068–5074.
- ²³⁵ Chen, M. S.; Lee, J.; Ye, H.-Z.; Berkelbach, T. C.; Reichman, D. R.; Markland, T. E. Data-efficient machine learning potentials from transfer learning of periodic correlated electronic structure methods: Liquid water at AFQMC, CCSD, and CCSD (T) accuracy. *J. Chem. Theory Comput.* **2023**,
- ²³⁶ Daru, J.; Forbert, H.; Behler, J.; Marx, D. Coupled cluster molecular dynamics of condensed phase systems enabled by machine learning potentials: liquid water benchmark. *Phys. Rev. Lett.* **2022**, *129*, 226001.
- ²³⁷ Liu, P.; Verdi, C.; Karsai, F.; Kresse, G. Phase transitions of zirconia: Machine-learned force fields beyond density functional theory. *Phys. Rev. B* **2022**, *105*, L060102.
- ²³⁸ Eckhoff, M.; Blöchl, P. E.; Behler, J. Hybrid density functional theory benchmark study on lithium manganese oxides. *Phys. Rev. B* **2020**, *101*, 205113.
- ²³⁹ Gillan, M. J.; Alfè, D.; Michaelides, A. Perspective: How good is DFT for water? *J. Chem. Phys.* **2016**, *144*, 130901.
- ²⁴⁰ Sauer, J. The future of computational catalysis. *J. Catal.* **2024**, *433*, 115482.
- ²⁴¹ Fu, X.; Wu, Z.; Wang, W.; Xie, T.; Ketten, S.; Gomez-Bombarelli, R.; Jaakkola, T. Forces are not enough: Benchmark and critical evaluation for machine learning force fields with molecular simulations. *arXiv preprint arXiv:2210.07237* **2022**,
- ²⁴² Kocer, E.; El Haouari, R.; Dellago, C.; Behler, J. Machine learning potentials for redox chemistry in solution. *arXiv preprint arXiv:2410.03299* **2024**,
- ²⁴³ Montero de Hijes, P.; Dellago, C.; Jinnouchi, R.; Schmiedmayer, B.; Kresse, G. Comparing machine learning potentials for water: Kernel-based regression and Behler–Parrinello neural networks. *J. Chem. Phys.* **2024**, *160*.
- ²⁴⁴ Omranpour, A.; Behler, J. A high-dimensional neural network potential for Co_3O_4 . *arXiv preprint arXiv:2409.11037* **2024**,
- ²⁴⁵ Yue, S.; Muniz, M. C.; Calegari Andrade, M. F.; Zhang, L.; Car, R.; Panagiotopoulos, A. Z. When do short-range atomistic machine-learning models fall short? *J. Chem. Phys.* **2021**, *154*, 034111.
- ²⁴⁶ Tkatchenko, A.; Scheffler, M. Accurate molecular van der Waals interactions from ground-state electron density and free-atom reference data. *Phys. Rev. Lett.* **2009**, *102*, 073005.
- ²⁴⁷ Becke, A. D.; Johnson, E. R. Exchange-hole dipole moment and the dispersion interaction. *J. Chem. Phys.* **2005**, *122*, 154104.
- ²⁴⁸ Becke, A. D.; Johnson, E. R. Exchange-hole dipole moment and the dispersion interaction revisited. *J. Chem. Phys.* **2007**, *127*, 154108.
- ²⁴⁹ Muhli, H.; Chen, X.; Bartók, A. P.; Hernández-León, P.; Csányi, G.; Ala-Nissila, T.; Caro, M. A. Machine learning force fields based on local parametrization of dispersion interactions: Application to the phase diagram of C_{60} . *Phys. Rev. B* **2021**, *104*, 054106.
- ²⁵⁰ Tu, N. T. P.; Rezajooei, N.; Johnson, E. R.; Rowley, C. N. A neural network potential with rigorous treatment of long-range dispersion. *Digit. Discov.* **2023**, *2*, 718–727.
- ²⁵¹ Grimme, S.; Antony, J.; Ehrlich, S.; Krieg, H. A consistent and accurate *ab initio* parametrization of density functional dispersion correction (DFT-D) for the 94 elements H–Pu. *J. Chem. Phys.* **2010**, *132*, 154104.
- ²⁵² Nielsen, M.; Björketun, M. E.; Hansen, M. H.; Rossmeisl, J. Towards first principles modeling of electrochemical electrode–electrolyte interfaces. *Surf. Sci.* **2015**, *631*, 2–7.
- ²⁵³ Levell, Z.; Le, J.; Yu, S.; Wang, R.; Ethirajan, S.; Rana, R.; Kulkarni, A.; Resasco, J.; Lu, D.; Cheng, J., et al. Emerging atomistic modeling methods for heterogeneous electrocatalysis. *Chem. Rev.* **2024**, *124*, 8620–8656.
- ²⁵⁴ Bonnet, N.; Morishita, T.; Sugino, O.; Otani, M. First-principles molecular dynamics at a constant electrode potential. *Phys. Rev. Lett.* **2012**, *109*, 266101.
- ²⁵⁵ Melander, M. M.; Kuisma, M. J.; Christensen, T. E. K.; Honkala, K. Grand-canonical approach to density func-

- tional theory of electrocatalytic systems: Thermodynamics of solid-liquid interfaces at constant ion and electrode potentials. *J. Chem. Phys.* **2019**, *150*.
- ²⁵⁶ Dufils, T.; Jeanmairet, G.; Rotenberg, B.; Sprik, M.; Salanne, M. Simulating electrochemical systems by combining the finite field method with a constant potential electrode. *Phys. Rev. Lett* **2019**, *123*, 195501.
- ²⁵⁷ Deußenbeck, F.; Freysoldt, C.; Todorova, M.; Neugebauer, J.; Wippermann, S. Dielectric properties of nanoconfined water: A canonical thermopotential approach. *Phys. Rev. Lett* **2021**, *126*, 136803.
- ²⁵⁸ Che, F.; Gray, J. T.; Ha, S.; Kruse, N.; Scott, S. L.; McEwen, J.-S. Elucidating the roles of electric fields in catalysis: a perspective. *ACS Catal.* **2018**, *8*, 5153–5174.
- ²⁵⁹ Léonard, N. G.; Dhaoui, R.; Chantarojsiri, T.; Yang, J. Y. Electric fields in catalysis: From enzymes to molecular catalysts. *ACS Catal.* **2021**, *11*, 10923–10932.
- ²⁶⁰ Christensen, A. S.; Faber, F. A.; Von Lilienfeld, O. A. Operators in quantum machine learning: Response properties in chemical space. *J. Chem. Phys.* **2019**, *150*.
- ²⁶¹ Gastegger, M.; Schütt, K. T.; Müller, K.-R. Machine learning of solvent effects on molecular spectra and reactions. *Chem. Sci.* **2021**, *12*, 11473–11483.
- ²⁶² Shao, Y.; Andersson, L.; Knijff, L.; Zhang, C. Finite-field coupling via learning the charge response kernel. *Electron. Struct.* **2022**, *4*, 014012.
- ²⁶³ Gao, A.; Remsing, R. C. Self-consistent determination of long-range electrostatics in neural network potentials. *Nat. Commun.* **2022**, *13*, 1572.
- ²⁶⁴ Zhang, Y.; Jiang, B. Universal machine learning for the response of atomistic systems to external fields. *Nat. Commun.* **2023**, *14*, 6424.
- ²⁶⁵ Joll, K.; Schienbein, P.; Rosso, K. M.; Blumberger, J. Machine learning the electric field response of condensed phase systems using perturbed neural network potentials. *Nat. Commun.* **2024**, *15*, 8192.
- ²⁶⁶ Weinberg, D. R.; Gagliardi, C. J.; Hull, J. F.; Murphy, C. F.; Kent, C. A.; Westlake, B. C.; Paul, A.; Ess, D. H.; McCafferty, D. G.; Meyer, T. J. Proton-coupled electron transfer. *Chem. Rev.* **2012**, *112*, 4016–4093.
- ²⁶⁷ Solis, B. H.; Hammes-Schiffer, S. Proton-coupled electron transfer in molecular electrocatalysis: theoretical methods and design principles. *Inorg. Chem.* **2014**, *53*, 6427–6443.
- ²⁶⁸ Hutchison, P.; Soudackov, A. V.; Hammes-Schiffer, S. Nonadiabatic proton-coupled electron transfer at a graphitic surface immobilized cobalt porphyrin. *ACS Catal.* **2024**, *14*, 14363–14372.
- ²⁶⁹ Akimov, A. V.; Muckerman, J. T.; Prezhdov, O. V. Nonadiabatic dynamics of positive charge during photocatalytic water splitting on GaN (10-10) surface: charge localization governs splitting efficiency. *J. Am. Chem. Soc.* **2013**, *135*, 8682–8691.
- ²⁷⁰ You, P.; Lian, C.; Chen, D.; Xu, J.; Zhang, C.; Meng, S.; Wang, E. Nonadiabatic dynamics of photocatalytic water splitting on a polymeric semiconductor. *Nano Lett.* **2021**, *21*, 6449–6455.
- ²⁷¹ You, P.; Chen, D.; Liu, X.; Zhang, C.; Selloni, A.; Meng, S. Correlated electron–nuclear dynamics of photoinduced water dissociation on rutile TiO₂. *Nat. Mater.* **2024**, *1*–7.
- ²⁷² Crespo-Otero, R.; Barbatti, M. Recent advances and perspectives on nonadiabatic mixed quantum–classical dynamics. *Chem. Rev.* **2018**, *118*, 7026–7068.
- ²⁷³ Westermayr, J.; Marquetand, P. Machine learning for electronically excited states of molecules. *Chem. Rev.* **2020**, *121*, 9873–9926.
- ²⁷⁴ Hu, D.; Xie, Y.; Li, X.; Li, L.; Lan, Z. Inclusion of machine learning kernel ridge regression potential energy surfaces in on-the-fly nonadiabatic molecular dynamics simulation. *J. Phys. Chem. Lett.* **2018**, *9*, 2725–2732.
- ²⁷⁵ Chen, W.-K.; Liu, X.-Y.; Fang, W.-H.; Dral, P. O.; Cui, G. Deep learning for nonadiabatic excited-state dynamics. *J. Phys. Chem. Lett.* **2018**, *9*, 6702–6708.
- ²⁷⁶ Dral, P. O.; Barbatti, M.; Thiel, W. Nonadiabatic excited-state dynamics with machine learning. *J. Phys. Chem. Lett.* **2018**, *9*, 5660–5663.
- ²⁷⁷ Westermayr, J.; Gastegger, M.; Menger, M. F.; Mai, S.; González, L.; Marquetand, P. Machine learning enables long time scale molecular photodynamics simulations. *Chem. Sci.* **2019**, *10*, 8100–8107.
- ²⁷⁸ Westermayr, J.; Gastegger, M.; Marquetand, P. Combining SchNet and SHARC: The SchNarc machine learning approach for excited-state dynamics. *J. Phys. Chem. Lett.* **2020**, *11*, 3828–3834.
- ²⁷⁹ Li, J.; Reiser, P.; Boswell, B. R.; Eberhard, A.; Burns, N. Z.; Friederich, P.; Lopez, S. A. Automatic discovery of photoisomerization mechanisms with nanosecond machine learning photodynamics simulations. *Chem. Sci.* **2021**, *12*, 5302–5314.
- ²⁸⁰ Axelrod, S.; Shakhnovich, E.; Gómez-Bombarelli, R. Excited state non-adiabatic dynamics of large photoswitchable molecules using a chemically transferable machine learning potential. *Nat. Commun.* **2022**, *13*, 3440.
- ²⁸¹ Meng, G.; Gardner, J.; Hertl, N.; Dou, W.; Maurer, R. J.; Jiang, B. First-principles nonadiabatic dynamics of molecules at metal surfaces with vibrationally coupled electron transfer. *Phys. Rev. Lett.* **2024**, *133*, 036203.
- ²⁸² Westermayr, J.; Faber, F. A.; Christensen, A. S.; von Lilienfeld, O. A.; Marquetand, P. Neural networks and kernel ridge regression for excited states dynamics of CH₂NH: From single-state to multi-state representations and multi-property machine learning models. *Mach. Learn.: Sci. Technol.* **2020**, *1*, 025009.
- ²⁸³ Eckhoff, M.; Behler, J. High-dimensional neural network potentials for magnetic systems using spin-dependent atom-centered symmetry functions. *npj Comput Mater* **2021**, *7*, 1–11.
- ²⁸⁴ Yuan, Z.; Xu, Z.; Li, H.; Cheng, X.; Tao, H.; Tang, Z.; Zhou, Z.; Duan, W.; Xu, Y. Equivariant neural network force fields for magnetic materials. *Quantum Front* **2024**, *3*, 8.
- ²⁸⁵ Bocus, M.; Goeminne, R.; Lamaire, A.; Cools-Ceuppens, M.; Verstraelen, T.; Van Speybroeck, V. Nuclear quantum effects on zeolite proton hopping kinetics explored with machine learning potentials and path integral molecular dynamics. *Nat. Commun.* **2023**, *14*, 1008.
- ²⁸⁶ Markland, T. E.; Ceriotti, M. Nuclear quantum effects enter the mainstream. *Nat. Rev. Chem.* **2018**, *2*, 0109.
- ²⁸⁷ Althorpe, S. C. Path-integral approximations to quantum dynamics. *Eur. Phys. J. B* **2021**, *94*, 155.
- ²⁸⁸ Kapil, V.; Behler, J.; Ceriotti, M. High order path integrals made easy. *J. Chem. Phys.* **2016**, *145*.
- ²⁸⁹ Cheng, B.; Behler, J.; Ceriotti, M. Nuclear quantum effects in water at the triple point: Using theory as a link between experiments. *J. Phys. Chem. Lett.* **2016**, *7*, 2210–2215.
- ²⁹⁰ Hellström, M.; Ceriotti, M.; Behler, J. Nuclear quantum

- effects in sodium hydroxide solutions from neural network molecular dynamics simulations. *J. Phys. Chem. B* **2018**, *122*, 10158–10171.
- ²⁹¹ Schran, C.; Briec, F.; Marx, D. Converged colored noise path integral molecular dynamics study of the Zundel cation down to ultralow temperatures at coupled cluster accuracy. *J. Chem. Theory Comput.* **2018**, *14*, 5068–5078.
- ²⁹² Cheng, B.; Engel, E. A.; Behler, J.; Dellago, C.; Ceriotti, M. Ab initio thermodynamics of liquid and solid water. *Proc. Natl. Acad. Sci. U.S.A.* **2019**, *116*, 1110–1115.
- ²⁹³ Schran, C.; Marx, D. Quantum nature of the hydrogen bond from ambient conditions down to ultra-low temperatures. *Phys. Chem. Chem. Phys.* **2019**, *21*, 24967–24975.
- ²⁹⁴ Schran, C.; Behler, J.; Marx, D. Automated fitting of neural network potentials at coupled cluster accuracy: Protonated water clusters as testing ground. *J. Chem. Theory Comput.* **2019**, *16*, 88–99.
- ²⁹⁵ Kapil, V.; Wilkins, D. M.; Lan, J.; Ceriotti, M. Inexpensive modeling of quantum dynamics using path integral generalized Langevin equation thermostats. *J. Chem. Phys.* **2020**, *152*.
- ²⁹⁶ Yao, Y.; Kanai, Y. Temperature dependence of nuclear quantum effects on liquid water via artificial neural network model based on SCAN meta-GGA functional. *J. Chem. Phys.* **2020**, *153*.
- ²⁹⁷ Yao, Y.; Kanai, Y. Nuclear quantum effect and its temperature dependence in liquid water from random phase approximation via artificial neural network. *J. Phys. Chem. Lett.* **2021**, *12*, 6354–6362.
- ²⁹⁸ Schran, C.; Briec, F.; Marx, D. Transferability of machine learning potentials: Protonated water neural network potential applied to the protonated water hexamer. *J. Chem. Phys.* **2021**, *154*.
- ²⁹⁹ Li, C.; Voth, G. A. Using machine learning to greatly accelerate path integral ab initio molecular dynamics. *J. Chem. Theory Comput.* **2022**, *18*, 599–604.
- ³⁰⁰ Kimizuka, H.; Thomsen, B.; Shiga, M. Artificial neural network-based path integral simulations of hydrogen isotope diffusion in palladium. *J. Phys. Energy* **2022**, *4*, 034004.
- ³⁰¹ Liu, L.; Tian, Y.; Yang, X.; Liu, C. Mechanistic insights into water autoionization through metadynamics simulation enhanced by machine learning. *Phys. Rev. Lett* **2023**, *131*, 158001.
- ³⁰² Plé, T.; Mauger, N.; Adjoua, O.; Inizan, T. J.; Lagardère, L.; Huppert, S.; Piquemal, J.-P. Routine molecular dynamics simulations including nuclear quantum effects: From force fields to machine learning potentials. *J. Chem. Theory Comput.* **2023**, *19*, 1432–1445.
- ³⁰³ Kwon, H.; Shiga, M.; Kimizuka, H.; Oda, T. Accurate description of hydrogen diffusivity in bcc metals using machine-learning moment tensor potentials and path-integral methods. *Acta Mater.* **2023**, *247*, 118739.
- ³⁰⁴ Kapil, V.; Schran, C.; Zen, A.; Chen, J.; Pickard, C. J.; Michaelides, A. The first-principles phase diagram of monolayer nanoconfined water. *Nature* **2022**, *609*, 512–516.
- ³⁰⁵ Lin, B.; Jiang, J.; Zeng, X. C.; Li, L. Temperature-pressure phase diagram of confined monolayer water/ice at first-principles accuracy with a machine-learning force field. *Nat. Commun.* **2023**, *14*, 4110.
- ³⁰⁶ Atsango, A. O.; Morawietz, T.; Marsalek, O.; Markland, T. E. Developing machine-learned potentials to simultaneously capture the dynamics of excess protons and hydroxide ions in classical and path integral simulations. *J. Chem. Phys.* **2023**, *159*.